

INFORMATION TO USERS

The most advanced technology has been used to photograph and reproduce this manuscript from the microfilm master. UMI films the text directly from the original or copy submitted. Thus, some thesis and dissertation copies are in typewriter face, while others may be from any type of computer printer.

The quality of this reproduction is dependent upon the quality of the copy submitted. Broken or indistinct print, colored or poor quality illustrations and photographs, print bleedthrough, substandard margins, and improper alignment can adversely affect reproduction.

In the unlikely event that the author did not send UMI a complete manuscript and there are missing pages, these will be noted. Also, if unauthorized copyright material had to be removed, a note will indicate the deletion.

Oversize materials (e.g., maps, drawings, charts) are reproduced by sectioning the original, beginning at the upper left-hand corner and continuing from left to right in equal sections with small overlaps. Each original is also photographed in one exposure and is included in reduced form at the back of the book.

Photographs included in the original manuscript have been reproduced xerographically in this copy. Higher quality 6" x 9" black and white photographic prints are available for any photographs or illustrations appearing in this copy for an additional charge. Contact UMI directly to order.

U·M·I

University Microfilms International
A Bell & Howell Information Company
300 North Zeeb Road, Ann Arbor, MI 48106-1346 USA
313/761-4700 800/521-0600



Order Number 1341274

Surface and aerosol models for use in radiative transfer codes

Hart, Quinn James, M.S.

The University of Arizona, 1990

U·M·I
300 N. Zeeb Rd.
Ann Arbor, MI 48106



**SURFACE AND AEROSOL MODELS
FOR USE IN
RADIATIVE TRANSFER CODES**

by

Quinn James Hart

A Thesis Submitted to the Faculty of the
COMMITTEE ON OPTICAL SCIENCES (Graduate)

In Partial Fulfillment of the Requirements
For the Degree of

MASTER OF SCIENCE

In the Graduate College

THE UNIVERSITY OF ARIZONA

1990

STATEMENT BY AUTHOR

This thesis has been submitted in partial fulfillment of requirements for an advanced degree at The University of Arizona and is deposited in the University Library to be made available to borrowers under rules of the Library.

Brief quotations from this thesis are allowable without special permission, provided that accurate acknowledgement of source is made. Requests for permission for extended quotation from or reproduction of this manuscript in whole or in part may be granted by the head of major department or the Dean of the Graduate College when in his or her judgment the proposed use of the material is in the interests of scholarship. In all other instances, however, permission must be obtained from the author.

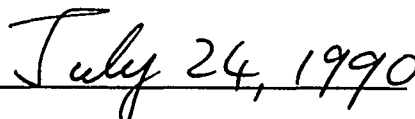
SIGNED: **APPROVAL BY THESIS DIRECTOR**

The thesis has been approved on the date shown below:



Dr. Philip N. Slater

Professor of Optical Sciences



Date

ACKNOWLEDGEMENTS

I would like to thank my wife Nicole for her support throughout my entire graduate study. She was my sympathetic ear, captivated audience, pillar of strength and source of motivation, all the while trying to complete her own degree. I would also like to thank my advisor, Dr. Philip N. Slater for guiding me through this masters degree. Special thanks also go to Dr. Stuart F. Biggar, Dave Gellman and the entire remote sensing group for their help, patience, and esprit de corps, which provided an atmosphere both educational and enjoyable. I am indebted to Dr. Ben Herman for his expertise in radiative transfer and atmospheric sciences. Without the previous six years of calibration studies, this work would have no foundation of data or methodology. I would also like to thank Dr. Richard D. McPeters, Dr. Arlin J. Krueger (NASA/GSFC), members of TOMS Nimbus Experiment and Ozone Processing teams, and the National Space Science Center for providing ozone data for White Sands Missile Range.

TABLE OF CONTENTS

	<u>Page</u>
LIST OF TABLES	5
LIST OF ILLUSTRATIONS	6
ABSTRACT	8
1. INTRODUCTION	9
2. THE REFLECTANCE-BASED CALIBRATION METHOD.	14
3. AEROSOL SIZE DISTRIBUTIONS	25
4. SURFACE REFLECTANCE MODELS.	34
5. RESULTS AND CONCLUSIONS	41
A. APPENDIX - CALIBRATION PROGRAM	61
REFERENCES	64

LIST OF TABLES

<u>Table</u>		<u>Page</u>
2.1	TM bandpasses	14
5.1	Predicted radiance values	42
5.2	Percent differences in radiance predictions	44
5.3	Linear fit slopes and intercepts	56

LIST OF ILLUSTRATIONS

<u>Figure</u>		<u>Page</u>
3.1	Comparison of size distribution for October 28, 1984	30
3.2	Predicted optical depths for October 28, 1984	31
3.3	Computed phase functions for October 28, 1984	32
3.4	Optical depth integrands	33
4.1	BRF measurements at 662 nm at White Sands Missile Range	37
4.2	BRF measurements at 826 nm at White Sands Missile Range	37
4.3	BRF measurements at 1658 nm at White Sands Missile Range	38
4.4	Polynomial fits to BRF for various solar zenith angles	39
4.5	Polynomial fits to BRF for various wavelengths	39
5.1	Counts per unit radiance for TM band 1	48
5.2	Counts per unit radiance for TM band 2	48
5.3	Counts per unit radiance for TM band 3	49
5.4	Counts per unit radiance for TM band 4	49
5.5	Counts per unit radiance for TM band 5	50
5.6	Counts per unit radiance for TM band 7	50
5.7	Diffuse to global ratios for TM band 1 on three calibration days	54
5.8	Diffuse to global ratios for TM band 2 on three calibration days	54
5.9	Diffuse to global ratios for TM band 3 on three calibration days	55
5.10	Diffuse to global ratios for TM band 4 on three calibration days	55
5.11	Linear estimations of counts per unit radiance for TM band 1	56

LIST OF ILLUSTRATIONS -- Continued

<u>Figure</u>		<u>Page</u>
5.12	Linear estimations of counts per unit radiance for TM band 2	57
5.13	Linear estimations of counts per unit radiance for TM band 3	57
5.14	Linear estimations of counts per unit radiance for TM band 4	58
5.15	Linear estimations of counts per unit radiance for TM band 5	58
5.16	Linear estimations of counts per unit radiance for TM band 7	59
A.1	Calibration overview	62

ABSTRACT

Absolute radiometric calibrations of Landsat 5 Thematic Mapper satellite are improved with the inclusion of a method to invert optical depth measurements to obtain an aerosol particle size distribution and a non-lambertian surface reflectance model. Also, a program is developed to improve speed and standardization of the entire calibration procedure.

The inverted size distributions can predict radiances varying from the previous jungian distributions by as much as 5 percent, though the reduction in the estimated error is less than one percent.

An empirical model for the surface reflection of White Sands using a two-degree polynomial fit as a function of scattering angle was employed. The model reduced estimated errors in radiance predictions by up to one percent.

Satellite calibrations dating from October, 1984 are reprocessed using the improved methods and a linear estimation of satellite counts per unit radiance versus time since launch is determined.

CHAPTER 1

INTRODUCTION

Absolute radiometric calibration of a satellite sensor is the process of assigning an absolute measure of radiance to the output digital counts. While many applications of the satellite imagery require only a relative measure of image radiances, there are some applications which require that the satellite be calibrated absolutely. These include determining ground reflectances from the satellite imagery, systematically removing sensor degradation from long term studies requiring comparison of scene radiance, and absolute measures of radiance levels for use as inputs into energy balance studies.

There are a number of methods to calibrate satellite sensors absolutely. One way is to use a calibrated source. This could be either an internal calibrator or the sun. For the internal calibrator the major assumption needed to provide an absolute calibration is that the source can be accurately characterized. This can be difficult as there is no way to determine changes in the source due to placing the sensor in space, and there is no way to chart the change of the source over time. Another disadvantage of using an internal calibrator or the sun is that it does not replicate the actual environment in which the sensor will be recording data. Stray light out of the field-of-view of the sensor is not accounted for with these sources. Often there is a considerable discrepancy between the radiances of the light used to calibrate the sensor and the radiance of the light in normal operation. This is especially true when using the sun as a calibration source.

An internal source normally cannot illuminate all of the light gathering optics, so the entire system cannot be calibrated. This last disadvantage can be used to advantage, however, when coupled with other calibration techniques. For example, when an internal calibrator that bypasses some of the optical path of the sensor is used in conjunction with another calibration which includes the whole optical system, it may then be possible to pinpoint more accurately the source of sensor degradation or other anomalies. Other advantages of an internal calibrator include its ease of use, an increased number of calibration opportunities, and its use as a check for other calibration techniques.

Other calibrations use calibrated targets rather than calibrated sources. These targets may be panels that are on-board the satellite, the moon, or selected parts of the earth's surface. On-board targets have similar problems as internal calibrators in terms of post-launch and temporal degradation of the target. Another problem with on-board targets as well as targets such as the moon is that the calibration procedures are not representative of how the sensor will be used to take measurements. This includes considerations of the field-of-view of the sensor and the stray light environment in which the sensor will be operating.

Methods of calibration which use the earth as a target have the immediate advantage that the calibration and acquisition modes of the sensor are very similar. One calibration method involves directly measuring the radiance leaving the atmosphere. This method involves flying over a target site with a calibrated spectroradiometer at the same time as the satellite overpass. The radiance that the radiometer records can then be used to determine the radiance at the satellite. Since the overflight with the radiometer is over most of the atmosphere, the correction for atmospheric attenuation is relatively minor. One problem with this method is the difficulty in replicating the satellite geometry with the spectroradiometer, as well as spatially

registering the measurements of the two sensors. Also, the spectral response of the two instruments should be matched. Other difficulties with the radiance calibration are its inconvenience and cost since the measurements cannot be made without flying over the target site.

The reflectance-based method is a procedure where the target surface reflectance is measured and the radiance at the sensor is predicted by using a computer code to model the radiative transfer of the light as it propagates through the atmosphere to the satellite. The radiative transfer program can predict both the direct contribution from the surface of the earth, and the diffuse radiance component, that is radiance directed into the sensor through multiple scattering events in the atmosphere alone, or deflected from surface reflections not in the field-of-view of the sensor. In theory, these predictions could be made for any type of atmospheric condition or surface reflectance distribution to accurately model any scene the sensor records. The disadvantage to this method is that in order to properly correct for the change in radiance at the satellite because of the atmosphere, it becomes necessary to characterize the atmosphere rigorously to complete the calibration. Therefore it becomes necessary to make many measurements that are used to more accurately model the atmosphere and not used directly in the calibration of the satellite. For parameters where measurements cannot be made, assumptions must be used. One advantage of the reflectance-based method is that most measurements are made at the target location. It is also possible to extract more information about the radiance at the sensor from a reflectance-based calibration. For example, it is possible to determine what fraction of incident radiance on the sensor is directly from the target, or what the radiance levels are out of the field-of-view of the sensor. Finally, this method very closely resembles the reflectance-retrieval algorithms that are used with the satellite data (Holm et al, 1989). Therefore, the algorithms used in the reflectance-based method are required for surface reflectance retrieval and any refinements made to the reflectance-based

calibration method can also be used as refinements to reflectance retrieval algorithms.

This thesis is concerned with enhancements to the reflectance-based calibration method. These consist first of an inversion method to determine the size distribution of the aerosol particles in the atmosphere, and second, the inclusion of non-lambertian surfaces. Both enhancements reduce the number of assumptions that have been previously made in satellite calibrations. A third development has been a separate computer program which helps to link and automate the steps involved in completing a calibration. This program increases the speed and consistency that calibrations can be performed.

Chapter 2 is an overview of the reflectance-based calibration method for the Thematic Mapper (TM) sensor system. There is an explanation of the steps involved in making a calibration, and a prediction of what effect the two enhancements will have on the calibration results.

Chapter 3 concerns the number density, or size distribution of the aerosol particles. In previous calibrations, the size distribution has been assumed to be juncian, which made computing the number density an easy task, related directly to the optical depth of the atmosphere as a function of wavelength. It also simplified the computation of the phase function for the ensemble of aerosol particles. A procedure in which aerosol optical depths are inverted to determine the number density will be discussed.

Another assumption made in previous calibrations is that the target surface is a lambertian reflector, that is the radiance of the surface is a constant, regardless of the viewing direction or the incident irradiance distribution. Chapter 4 describes replacing the lambertian assump-

tion with an empirical model of the surface reflectance.

In Chapter 5, all previous reflectance-based Thematic Mapper calibrations are reprocessed with these enhancements and comparisons are made with the previous calibrations. They are also compared with the previous results of the internal calibrator. Code predictions of the ratio of diffuse radiance to direct irradiance are compared to actual measurements where that data are available. The results of these comparisons are used to judge the importance of these enhancements and determine whether or not they are necessary to obtain the accuracy that is desired in the absolute calibration of the satellite sensors. One error budget (Biggar, 1990) for a satellite calibration, predicts that errors of 2 percent can result from uncertainties in the number density, and 1.2 percent from a lambertian surface assumption.

Further measurement enhancements that should be made to decrease the errors and other possible methods for retrieving more information will be discussed.

CHAPTER 2

THE REFLECTANCE-BASED CALIBRATION METHOD

The reflectance-based method of calibration can be used conveniently for satellite sensor systems that operate in the solar reflective spectral range and have instantaneous fields-of-view of less than 50 meters. The emphasis for this study was TM, which is a whiskbroom type satellite sensor that orbits the earth at 705 km, and repeats global coverage every 16 days. The sensor has seven spectral bands, six of which are in the solar reflective range and are considered here. The bandpasses for the six bands of interest as determined by the moments method, Palmer (1984), are shown in Table 2.1. The calibrations were performed at White Sands Missile Range in New Mexico, which offers large, bright targets that are uniform to a good degree and offer a surface displaying lambertian qualities over a large range of angles. The satellite nadir viewing angle was less than 7 degrees for all calibrations with solar zenith angles varying about an average of 45 degrees.

Table 2.1 : Thematic Mapper bandpasses

TM Band	Bandpass (μm)	Central (μm)
1	0.45 - 0.52	0.4863
2	0.52 - 0.60	0.5706
3	0.63 - 0.69	0.6607
4	0.76 - 0.90	0.8382
5	1.55 - 1.75	1.6770
7	2.08 - 2.35	2.2230

The reflectance-based method involves measuring the reflectance of the target to be used for the calibration, characterizing the atmosphere, and then running a radiative transfer code to predict the radiance at the sensor. Once the radiance at the sensor is known, a simple com-

parison can be made against the digital counts that were recorded by the satellite while it viewed the target. Assuming a linear response and a known offset will allow the counts per unit radiance to be determined.

The radiative transfer code used for these calibrations was developed by Herman (1963). It divides the atmosphere into homogeneous plane-parallel layers. The width of the layers are determined such that approximately 96 percent of the scattering events that take place in each layer are single scatter events. The entire zenith and azimuth ranges are divided into a number of sections, and the scattering into each section is calculated. The code runs iteratively to reach a solution that predicts the radiance at each level and for each section. Each layer of the modeled atmosphere can have different atmospheric pressures and different concentrations of water vapor, ozone, aerosols and other gases. In the ideal case all inputs to the radiative transfer code are completely known, that is, there is enough information to completely describe the environment which the sensor is viewing. The radiative transfer code predicts not only the radiance at the sensor, but at the surface as well. These results could be compared to actual ground-based measurements to validate the code predictions.

Most of the uncertainties of the reflectance-based method come from the fact that the input parameters to the radiative transfer code are not known ideally. In actual calibrations, gaseous concentrations and vertical profiles are assumed to follow various models. The concentration and makeup of the aerosol particles must also be assumed or derived from ground based methods. The reflectance of the surface cannot be predicted completely, and measurements of the surface reflectance, especially in situ, are not complete. The scattering and absorption of light due to particles is analytically known only for simple particle shapes like spheres. This means that one input to the radiative transfer code, the phase function of the aerosol

particles, cannot be calculated for aerosol particles of complicated or irregular shapes, and these particles must be assumed to be spherical.

Two parameters which cause a sizable change in the radiance prediction are the size distribution of the aerosol particles, and the reflectance of the surface. The purpose of this thesis is to model these two parameters more accurately to improve the predictions of the radiative transfer code.

A change in the size distribution of the aerosol particles can affect the predictions of the radiative transfer code in three ways. First, a change in the distribution can change the predicted values for the optical depths at the sensor bandpasses. Second, different distributions can produce changes in the percentages of light scattered and absorbed. This means that while two distributions may extinguish the same amount of light from the direct solar irradiance, one distribution may scatter more light. This predicts an increase in diffuse radiance which would increase the radiance predicted both at the surface and at the sensor. Third, different size distributions will also affect the shape of the phase function, which can also affect the radiance predictions.

Previous calibration attempts modeled the aerosol particles with a jungian size distribution. In Chapter 3, a distribution obtained from inverting optical depth measurements is discussed. The only assumption on the distribution is that it is smooth. The chapter shows what affects the different distributions can have on calibration procedures. Chapter 5 uses this new method of size distribution determination and compares the results of actual calibrations using the jungian assumption to the number density inversion.

It is of interest to note the magnitude of the amount of light extinguished by the aerosol particle distribution as compared to the amount of light scattered by the Rayleigh scattering of the air molecules and the absorption of light by various gases. We will consider average conditions at White Sands Missile Range when the sun is nearly directly overhead. Near the low end of the visible spectrum, at $0.5 \mu\text{m}$, gases absorb 1-2% of the solar irradiance as it propagates through the atmosphere. The air molecules will scatter about 15% of the irradiance out of the direct path. The aerosol particles will attenuate about 15% of the irradiance as well, though only 80-90% will be scattered, the rest will be absorbed. As the wavelength increases out into the IR, to $2 \mu\text{m}$, then the aerosol extinction is much greater than the Rayleigh scattering. Both of these fractions are much less however. The gaseous absorption is on the order of 5%, but the Rayleigh scattering has now reduced to about 0.1% and the extinction by the aerosol particles is less than 1%. The shorter wavelengths, therefore, are where any changes as a result of a change of size distribution would be expected to be most noticeable.

Another assumption that was made for the previous calibrations was that the surface was a lambertian reflector. A lambertian reflector is a surface which reflects the same amount of radiance into every angle regardless of the distribution of incident radiance. The reason the lambertian assumption is appealing when modeling the surface reflection is because the entire surface can be modeled with a single value. Also, rather than having to calculate the reflection separately for all incident radiance, the sum of the incident radiance can be multiplied by a single factor to obtain the radiance scattered into every angle. For some surfaces, like parts of the White Sands Missile Range, where the TM calibrations took place, the lambertian assumption holds relatively well when the angle between the incident and exitant directions is less than ninety degrees. For most other surfaces, the lambertian assumption fails more dramatically.

To model the reflectivity of a surface more accurately than the lambertian assumption, it is necessary to determine the bidirectional reflectance distribution function or BRDF. The BRDF is the ratio of exitant radiance at any given zenith and azimuthal angles to an irradiance beam incident on the surface.

$$\text{BRDF or } f(\theta, \phi; \theta', \phi') = \left(\frac{dL(\theta, \phi; \theta', \phi')}{dE(\theta, \phi)} \right)_{\text{sr}^{-1}} \quad (2.1)$$

Where dL is the exitant radiance in an incremental solid angle with zenith angle θ' and azimuth angle ϕ' , and dE is the incident plane-parallel radiation from a direction with zenith angle θ and azimuth angle ϕ (Slater, 1980).

The direct solar flux impinges on the surface as plane-parallel radiation, and therefore the BRDF is immediately applicable. For the diffuse component, however, which is a radiance distribution, an incident irradiance is computed by multiplying the incident radiance by an incremental solid angle. To compute the total reflected radiance then, the incident radiance times the BRDF is integrated over the entire hemisphere. Another measure of the surface reflectance is the bidirectional reflectance factor, or BRF, which is simply the ratio of BRDF of the surface to the BRDF of a lambertian reflector. This ratio can be measured and demands no knowledge of the incident irradiance unlike the BRDF.

The assumption of a lambertian surface reflection assumption only correctly models the reflectance of the direct solar irradiance into the direction of the sensor. This is the reflectance measured and the surface is then assumed to be lambertian with this value as its reflectance factor. A non-lambertian surface reflection model will affect the predictions of the radiative transfer code through multiple scattering events. These include the reflection of the diffuse radiance component at the surface into the direction of the sensor, the reflection of the direct irradiance in other directions which are then scattered back into the sensor field of view, and

other multiple scatter events. For the surface at White Sands, the reflectance varies from lambertian by only 10% for angles up to 90 degrees. The maximum variation from lambertian is at very glancing angles and can be 170% of the lambertian prediction.

Following this discussion on the reflectance-based method, including the refinements to be made on the previous calibrations, it is worthwhile to summarize all the assumptions that are needed to complete a calibration, as well all the measurements that are made. Most of the assumptions are based on some underlying physics about the parameter, or previously obtained models. Many of the assumptions that are made pertain to the atmosphere.

- The atmosphere is temporally stable - This must be assumed because determination of the optical depth as a function of wavelength is performed using the Langley method. This method involves taking measurements throughout the day and then assuming the atmosphere was the same for every data point. Another reason to assume temporal stability is to allow for the inclusion of measurements that were taken at times other than the time of the overpass.
- The atmosphere is horizontally homogeneous - This is a necessary assumption because the radiative transfer code assumes that the atmosphere varies only with height.
- The atmosphere is a series of plane layers - In reality, even if the atmosphere did not change in the horizontal direction, it would instead be a series of spherical shells rather than plane layers. The plane layer assumption is to allow for an easier implementation of the radiative transfer code. This assumption makes very little difference until the angles of interest are near the horizon which is never the case in the sensor calibrations.
- The vertical profiles of the atmospheric constituents are known - Vertical profiles of the aerosol particles, ozone concentration, pressure and temperature, and water vapor are all required. All are assumed to follow models for a generic atmosphere. The total

concentrations of these are measured, and then the vertical profiles scaled to give the appropriate amounts.

There are also many assumptions that are made about the aerosol particles in the atmosphere.

- All aerosols are spherical - Without this assumption Mie theory could not be used to predict the scattering of the particles.
- The size distribution is smooth - The previous assumption of a juncian distribution has been replaced by an inverted distribution which assumes the distribution is smooth.
- The relative size distribution is constant with height - This assumption assumes that at different altitudes, only the number of particles change and not the relative size distribution. This allows for a single distribution to model the entire atmosphere.
- The size limits for the particles are known - This assumption can be troublesome and is discussed further in chapter 3.
- All aerosols have the same index of refraction, this index is known exactly, and this index is non-dispersive, that is it is constant with respect to wavelength - There are of course many different possibilities for the aerosol particles. There could be more than one type of particle, each with a separate index of refraction, including dispersion. Another possibility is that the particles, rather than being of a constant index, would be treated more accurately as a sphere of one index coated with material of another index. One possibility for this is that the particles are coated with a film of water. This coating could then be a function of the relative humidity and of the temperature, and therefore, the same particles would vary from height to height and day to day depending on the water vapor content. The representative index used in White Sands calibrations was chosen to be $m = 1.44 - 0.005i$ (Herman, 1987) (Santer, 1987).

Because of all the assumptions that are made about the aerosol particles, the term "effective" aerosols is often used. The meaning of this is that although the aerosol particles are probably made up of a number of different constituents with varying indices, distributions and shapes, the scattering from this ensemble of particles can be represented reasonably well by another distribution of particles, all spherical and all of a constant index. These then are the effective aerosols. The advantage of using the effective particles is that they are much easier use in determining a phase function. Also, the size distribution is inferred from measurements, and it would be impossible to make this determination if the index and shape of the particles were not assumed to be known. The major disadvantage of using an effective ensemble of particles is that it becomes very difficult to include independent measurements of the aerosols into the determination of the particles. For example, if it were known that all the particles were of a certain index but also that they were cubes rather than spheres, then it would be impossible to include the knowledge of the index without including also the shape of the particles. But since there is no analytic solution for cubes particles, they still must be assumed to be spheres. With this assumption, we then assume that the actual index is the best estimate of the effective particle index and not that some other index would give closer agreement to the actual scattering of the particles.

There are some assumptions that have to be made about the surface of the calibration site as well.

- The surface is homogeneous - This allows for the surface BRF to be measured at one point and the results used for the entire surface. Because of a homogeneous surface there can be no surround effect, that is an effect where the actual target appears brighter or darker because of being surrounded by a brighter or darker surface. This assumption is good for the calibration site chosen, since the surface is very uniform and

is at the center of a 30 km diameter area of roughly the same reflectance.

- The surface reflectance is rotationally symmetric - This assumption is necessary for the modeling of the surface BRDF. The surface reflectance will be assumed to be a function of the scattering angle between the incident and exitant directions. This is an improvement over the prior assumption that the surface was a lambertian reflector.

There is another assumption that concerns the polarization of the light. When light is scattered or reflected from a surface there is a change in its polarization. How the light is scattered and reflected is also dependent on the polarization of the incident beam. Since the radiative transfer code used only determines the total intensity scattered in any direction, and also the incident intensity is always assumed to be unpolarized, the assumption is made that the scattering by aerosol particles depolarizes the light polarized by Rayleigh scattering. For an atmosphere with no aerosol particles, inclusion of polarization effects can change the predicted radiance at the sensor by up to 2%.

After considering all the assumptions that must be made on the parameters of the radiative transfer code, we will now look at all the measurements that are made to determine some parameters and to complete the calibration of the sensor.

- The direct solar irradiance as a function of airmass - This measurement is made to determine the optical depth by the Langley method. This is a method where optical depth is determined from the change in attenuation of the solar irradiance due to the change in the length of the path that the irradiance travels through to reach the surface.
- Sensor digital counts - The digital counts from the sensor while it was viewing the site are needed to make the final comparison of radiance at sensor verses digital counts.

- **Air pressure** - The air pressure is measured to determine magnitude of Rayleigh scattering.
- **Overpass time** - The time of overpass is used to determine the geometry of the sun and the sensor at the time of overpass for inclusion into the radiative transfer code.
- **Ozone concentration** - There must also be a method for determining the amount of ozone that is present. It is sometimes possible to obtain an independent measure of ozone. The TOMS sensor, or Total Ozone Mapping Spectrometer, produces daily maps of the ozone concentrations for the entire globe. The TOMS data are not immediately available so other methods of ozone determination are sometimes needed. These methods normally begin with optical depth data as a function of wavelength, corrected for Rayleigh scattering so that, they are due only to the aerosol particles and the ozone absorption. An iterative routine is then carried out to determine what concentration of ozone combined with the aerosol contribution produces optical depths closest to those measured. The problem with this is that it involves assumptions on the aerosol optical depths and therefore on the size distribution. Since a relatively large change in ozone concentration results in a relatively small change in the transmittance due to the ozone, it is sufficient to assume amount of ozone as a function of the time of year.
- **Water vapor** - The relative humidity and temperature are also measured. These measurements, combined with vertical profile models can be used to estimate the amount of water vapor as a function of height. This is used to determine the amount of attenuation of the light due to absorption by the water vapor.
- **Surface reflectance** - Finally, measurements of the surface reflectance are taken. When it is assumed that the the surface is a lambertian reflector, only one measurement is necessary to characterize the surface. For a less restrictive reflectance model, more measurements must be taken. Chapter 4 is a detailed description of the measurements

made and the model formulated.

In order to improve the calibration technique, a program was written which increases the speed and consistency of the entire procedure. Basically, this calibration program allows the user to enter in pertinent data into the computer program in a simple way. The program then writes the input files needed for various data reduction codes, and creates a batch file to run these codes. The result is that the user obtains the output files of interest in a consistent manner without the errors introduced in manually performing these tasks. The program does not improve the speed of the data reduction codes, but eliminates manual preparation of the data. It increases the speed in performing calibrations, reduces errors in data entry, and standardizes the output files created by the other codes. Appendix A contains a flowchart of the calibration computer programs and a description of the new code.

CHAPTER 3

AEROSOL SIZE DISTRIBUTIONS

In order to determine the scattering and absorption of an ensemble of aerosol particles of different sizes, shapes, or indices, it is necessary to sum the properties of all particles to obtain a single phase function for the entire ensemble. If we assume that the particles are spheres, so that we may use Mie theory to compute the scattering, and that they are all of the same index of refraction, then it is only necessary to integrate the phase function for each radius, weighted by the number of particles of each size, over all radii. Though actual aerosol particles do not are not required to follow any functional form, there have been a few empirical equations used to attempt to model the number density of aerosol particles. One of the simplest forms is the jungian size distribution which states that the number of particles per unit interval in r is

$$n(r) = Cr^{-(\nu+1)} \quad (3.1)$$

where C is a constant and ν is known as the jungian parameter. Another implicit assumption about the jungian distribution is that the possible radii values extend from 0 to ∞ . The derivation of the jungian size distribution follows from the fact that often the optical depths due to the aerosols vary almost linearly in log space. The jungian distribution predicts this, and allows for evaluation of the jungian parameter directly from the optical depth measurements.

It is also possible to invert the measurements of the optical depth as a function of wavelength in order to determine the size distribution of the aerosol particles. This requires no assumption that the distribution follow any specified functional form, but in order to extrapolate the results to all radii values requires an assumption as to the smoothness of the distribution. This

method was used to relax some of the assumptions for determining the phase function.

The starting point for both of these distributions is the equation for the aerosol optical depth. If we assume that the particles have a non-dispersive index, m , that the number of particles per unit interval in radius, r , and height, z , is given by $n(r, z)$, and that the particles are spherical with an extinction cross section of Q_{ext} , as obtained through Mie theory, then the aerosol optical depth can be written as

$$\delta_a(\lambda) = \int_0^{z_t} dz \int_0^{\infty} dr Q_{ext}(r, \lambda, m) \pi r^2 n(r, z) \quad (3.2)$$

where z_t indicates the top of the atmosphere. It is then possible to carry out the height integration to determine a function, $n_c(r)$, which is the size distribution of the particles taken over the entire atmospheric column. This reduces δ_a to an integration over r alone. Further it is necessary to integrate r only over values where $n_c(r)$ is not equal to zero, from the minimum to the maximum radii in the size distribution.

$$\delta_a(\lambda) = \int_{r_n}^{r_x} dr \pi r^2 Q_{ext}(r, \lambda, m) n_c(r) \quad (3.3)$$

- r = radius of particles
- λ = wavelength
- m = complex index of refraction
- $Q_{ext}(r, \lambda, m)$ = extinction efficiency
- $n_c(r)$ = columnar aerosol size distribution
- r_n = minimum radius of $n_c(r)$
- r_x = maximum radius of $n_c(r)$

Having reached this point, it is now possible to see why the jungian size distribution is so appealing as an approximation to the number distribution. If we assume a jungian distribution with integration limits of 0 and ∞ , then the Mie optical depth is

$$\delta_a(\lambda) = \int_0^{\infty} dr \pi r^2 Q_{ext}(r, \lambda, m) C r^{-(\nu+1)} \quad (3.4)$$

Where C is the constant for the jungian distribution integrated over height. Using the fact that the extinction efficiency is a function only of the ratio of the radius and the wavelength, and making the change of variables to the size parameter, $x = \frac{2\pi r}{\lambda}$ we obtain

$$\delta_a(\lambda) = C \pi \left(\frac{\lambda}{2\pi} \right)^{-(\nu-2)} \int_0^{\infty} dx Q_{ext}(x, m) x^{-(\nu-1)} \quad (3.5)$$

and since the integral is merely another constant

$$\delta_a(\lambda) \propto \lambda^{-(\nu-2)} \quad (3.6)$$

Therefore a jungian size distribution can be determined directly from optical depth measurements as a function of wavelength, except for a multiplicative constant. There is a linear relationship between the optical depth and the wavelength in log space with the jungian parameter directly related to the slope.

Equation 3.3 is also a good starting point in explaining how the optical depth measurements can be used to invert for the columnar size distribution. The determination of the size distribution then is an inversion of a number of integrals, for different wavelengths, λ , with the extinction cross section of the aerosol particles as the kernel functions. Note that it is not necessary that the index of refraction be non-dispersive for this procedure to be valid. In practice, the non-dispersive index is attractive because then a single function for Q_{ext} can be used for all wavelengths and only scaled differently for each wavelength. The idea then is that from a number of different measurements of the optical depths, the underlying size distribution can be determined. The inversion of optical depth measurements to obtain a size distribution was discussed by King (1978) and a modified version of the code developed there was used for the inversions used in the calibrations of TM. For a description concerning the

inversion procedure the reader is encouraged to refer to King's paper.

One consideration of the inversion procedure is the limits of the particle radii. The estimation of the limits is based on both the underlying physics of aerosol particles and the effect that the limits have on the solution. The choice of radius maximum has little effect on the phase function because there are so few of the larger particles. Therefore, a choice of $5 \mu\text{m}$ as a maximum radius value gives a very similar result to an inversion with a maximum of $10 \mu\text{m}$. The lower bound of the radius interval can have a much greater effect on the outcome of the inversion. This can be expected because most size distributions are at least similar to a juncian distribution which predicts that the greatest number of particles are in the smallest radii ranges. Therefore, moving the minimum radius value has the effect of allowing or disallowing a large number of particles.

One way to estimate the effect of the minimum radius choice is to run the inversion routine to compute a size distribution, then plot the integrand of equation 3.3 which determines the optical depth for a given wavelength. If the contribution to this integral is small from the lowest radii particles then the inversion is likely to be somewhat insensitive to the choice of the minimum radius. If a large contribution to the integral is in the minimum radius range, however, the inversion is likely to be very dependent on the choice of the minimum radius. For the TM calibrations, the lower bound was chosen to be $0.05 \mu\text{m}$ for all cases. King discusses the choice of the minimum radius parameter in more detail, and concludes that some experimentation with the minimum radius limit would perhaps net some better results. King also discusses the sensitivity of the inversion routine to the index of refraction chosen for the particles and to the initial guess for the size distribution.

Figure 3.1 shows the results of an inversion using actual data from a calibration. The inverted size distribution is shown along with the computed best-fit jungian distribution for the same data. This is an example of what would be considered a well-behaved inversion. The number distribution tails off at both ends of the radius endpoints indicating that the choice of endpoints is not critical to the solution. Using the size distribution from the inversion routine rather than the best-fit jungian distribution can affect the radiative transfer for the TM calibrations in three ways. First, each distribution will predict different optical depth values for the TM bands. This is most notable when computing the optical depth calculations beyond the longest wavelength measurement. How much the dissimilarities of the distributions affect the results of the optical depths can be seen in figure 3.2. This graph shows the predicted optical depth measurements from both size distributions. Once the number distribution is determined, the optical depth at any wavelength can be calculated. Figure 3.2 shows the predicted optical depths at the central wavelength for each TM band. It can be seen that the predictions for each can vary from one another quite substantially. However, for the longer wavelengths, the optical depths are so small that the change in optical depth brings about only a small change in the predicted radiance at the sensor.

The second way that the size distributions can affect the radiative transfer code is in the shape of the phase function that is predicted by each. Once the size distribution is known, it is possible to determine the phase function of the aerosol particles due to the distribution. The phase function for the entire size distribution is computed in a manner similar to the computation of the optical depths. In this case, however, the amount of scattering is a function of the scattering angle.

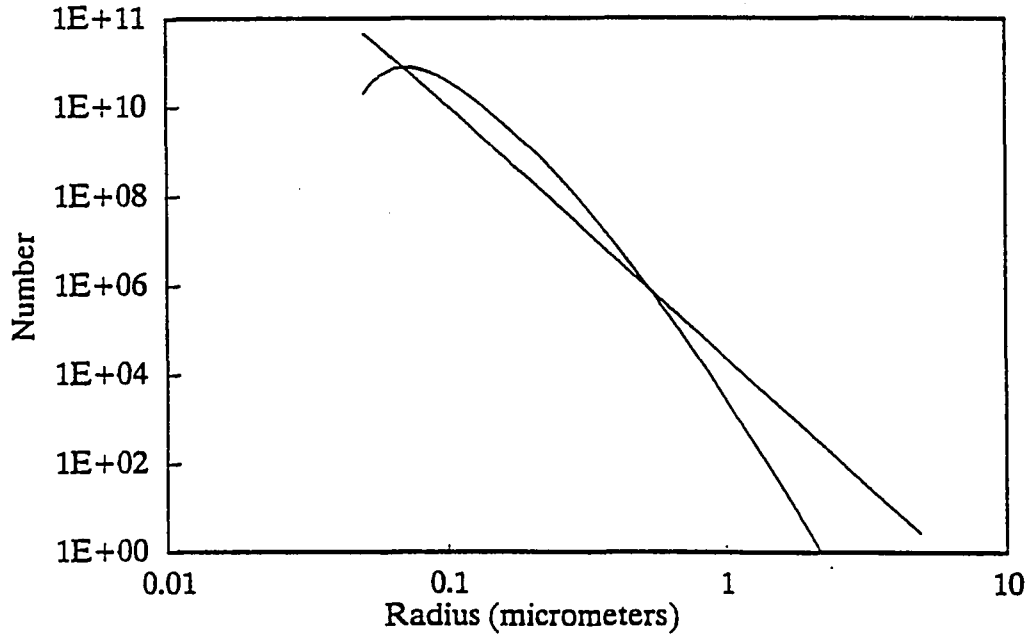


Figure 3.1 : Comparison of inverted number distribution and the straight line best-fit jungian distribution for October 28, 1984 at White Sands Missile Range.

$$S(\lambda, \Theta) = \int_{r_n}^{r_x} dr s(r, \lambda, m, \Theta) n_c(r) \quad (3.7)$$

where $S(\lambda, \Theta)$ is the scattering through any angle, Θ , at any wavelength, λ , due to the entire ensemble of particles, and $s(r, \lambda, m, \Theta)$ is the scattering through any angle by a single particle of radius r , index m , and wavelength λ . Mie theory is actually more specific than this, predicting the scattered radiance intensity and polarization characteristics given the incident polarization characteristics. The complete Mie theory was not used in the radiative transfer model because the inclusion of polarization of the scatterers increases the complexity of the model by a factor of sixteen, and is very dependent on the shape of the particles if they are not spherical. Figure 3.3 shows the phase function predicted by both distributions for two different wavelengths. It can be seen that the shape is different for each distribution. The difference in shape is greater in the longer wavelengths, as was the change in the optical depth due

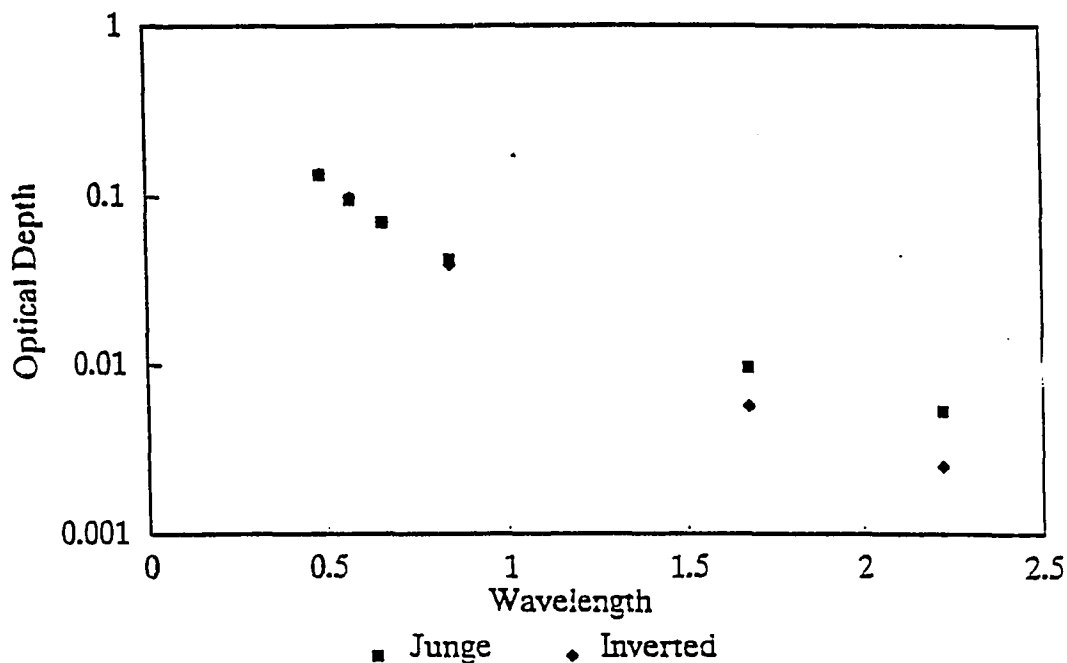


Figure 3.2 : Graph of optical depth predictions using both distributions of October 28, 1984, at the TM band central wavelengths.

to each distribution. The total amount of scattering in the longer wavelengths, however, is much less than in the shorter ones.

The third way in which the different size distributions can affect the results is in terms of their respective predictions of the percentage of extinguished light that is scattered rather than absorbed. Figure 3.3 shows the scattering for the two distributions as a function of angle. It is difficult to see from this graph, however, that one distribution predicts the total amount of scattered light to be greater than the other. The amount of light that is scattered per unit area by the column of aerosol particles can be described by the scattering cross section for the entire distribution. This value can not be measured directly, but can be predicted using Mie theory. The ratio between the scattering cross section and the extinction cross section is known as the single scattering albedo. A change in this value will bring about a change in the

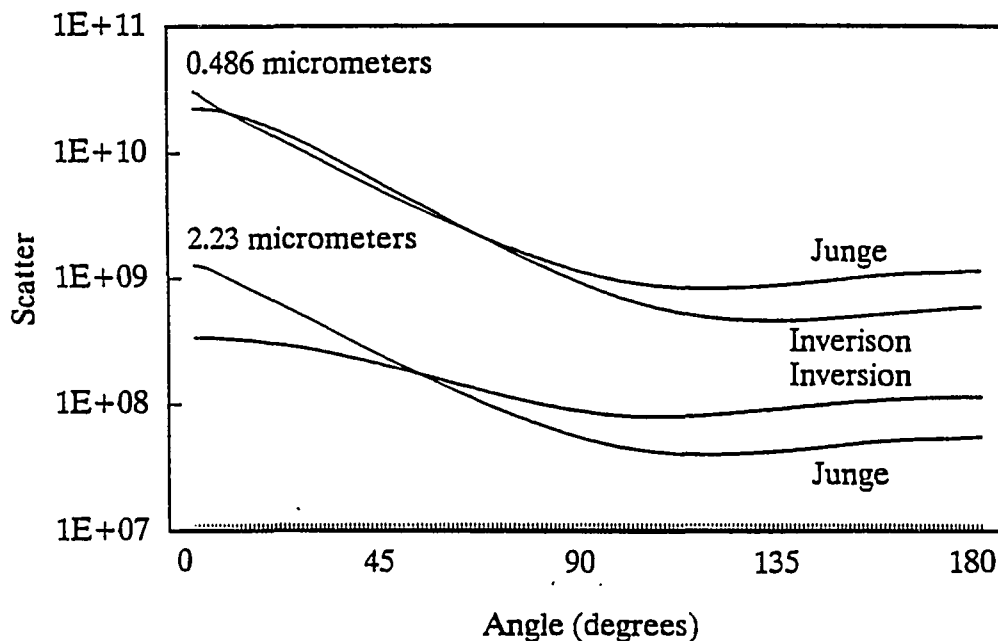


Figure 3.3 : Calculated phase function for the two size distributions at wavelengths of $0.486 \mu\text{m}$ and $2.23 \mu\text{m}$. Besides showing the difference in phase function due to the different distributions, the graph shows that for longer wavelengths, the amount of scattering is much less.

amount of diffuse radiance that is present at the surface of the earth, even if the extinction is the same. This diffuse component can have a large affect on the predictions of the radiance at the sensor. The fact that the different distributions can have different single scattering albedos is possible because of the radius range that drives the distributions. Figure 3.4 shows the graph of the integrand of equation 3.3 used to determine the optical depth, or extinction cross section. integrand for the computation of the scattering cross section is shown as well. From this graph it can be seen that the particles near chosen endpoints of 0.05 and $5 \mu\text{m}$ do not contribute to the optical depth greatly. This means the results are somewhat insensitive to the radii choices, though increasing the minimum to $0.1 \mu\text{m}$ or beyond would affect the jun-gian distribution. It can also be seen that the radii values which really drive the integral occur at different values for the different size distributions. These differences in size distribution

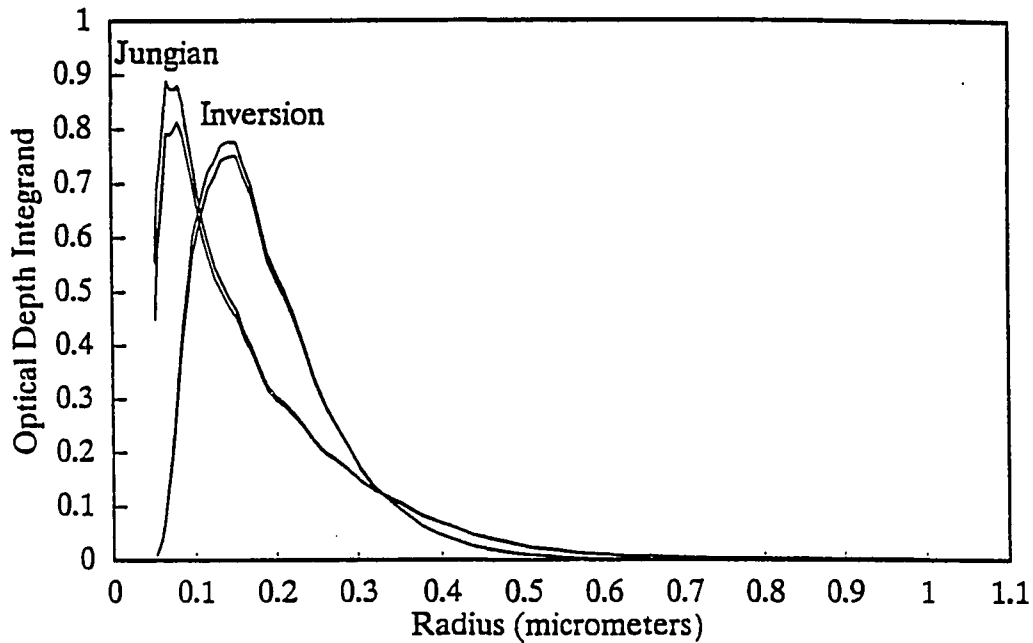


Figure 3.4 : Graphs of extinction and scattering integrand for both distributions of October 28, 1984, showing which radius range drives optical depth determinations. The data are for the determination of the optical depth at $0.486 \mu\text{m}$.

weight the individual single scattering albedos differently and as a result the single scattering albedo for the ensemble of particles can be quite different. Though the scattering and extinction cross sections can not be measured directly, they directly affect the ratio of diffuse to direct irradiance at the surface. Therefore, the radiative transfer code predictions of this ratio can be used as a test of the validity of the size distribution.

In Chapter 5 the results of recomputing all previous calibrations using both the best fit jungian distribution and the size distribution predicted by the inversion procedure are presented. Any differences in the calibrations for each day due to this change will be shown and discussed. Also, the predicted ratio of diffuse to direct irradiance will be compared to actual measurements for days when the measurements are available.

CHAPTER 4

SURFACE REFLECTANCE MODELS

The surface reflectance is important in predicting the radiance leaving the surface. This radiance is a combination of the reflected direct solar irradiance and the reflected diffuse radiance. In the previous calibrations of TM the method for modeling the surface reflectance was to assume that the ground was a lambertian reflector and then measure the reflectance in the sensor direction during overpass. This method insured that the major surface reflectance event, that is the reflectance of the direct irradiance in the direction of the sensor was modeled correctly.

The reasons that a single value reflectance factor can fail to describe the reflectance relate to both the direct and the diffuse radiance fields incident on the surface. First, because the surface is not lambertian, the radiance reflected from the direct field into angles other than the sensor look angle will not be modeled correctly. This can affect the radiance at the top of the atmosphere in the direction of the sensor due to multiple scattering events that introduce radiance from the different angles back into the direction of the sensor view. Second, the diffuse component of the incident light will not reflect off the surface the same way that the direct component will, due to the different scattering geometries. In the shortest wavelength TM band for a standard White Sands atmosphere, the diffuse component can be as much as 25% of the incident light on the surface, though the longest TM bands may only have a 1% diffuse component.

There are many possible ways to model the BRF of a surface. One method would be to measure the BRF at a number of different incident and exitant angle combinations and to store these values in a large table. The radiative transfer code could then use this table to look up any desired BRF to model the surface reflectance. Another method would be to derive an empirical model which fits the measured data reasonably well. The problem with an empirical model in the general case is that it would be a function of four angle parameters and for some surfaces fitting a functional form to the BRF would be quite difficult. In these cases a tabulated look-up table would be a better solution.

When certain assumptions can be made about the surface, however, the empirical model can be simplified. The first assumption that can be made is that the surface is rotationally symmetric. This means that the surface reflectance is a function only of the two zenith angles and of the azimuthal angle difference of the incident and exitant directions. Bare soil or asphalt are examples where this assumption is valid. This assumption removes one parameter from the empirical model. The next possible assumption is that the BRF is a function only of the angle between the incident and exitant direction in the plane containing both these rays, sometimes referred to as the scattering angle. This reduces the empirical model from three parameters down to one, the angle between the incident and exitant directions. If this assumption is valid, the empirical method has the advantage over the tabulated method in terms of simplicity and absence of redundancy. For the surface reflectance measurements of White Sands Missile Range, an empirical formula as a function of scattering angle could describe the surface adequately.

Regardless of the method used to determine the BRF of the surface, measurements must be made at the surface to derive the model. There are difficulties in making BRF measurements.

If the measurements are taken during the day with the sun as the source, then the only possible incident azimuthal and zenith angles are those that the sun will occupy in the course of the day. Also, a method must be used to separate the contribution to the reflected radiance from the direct plane parallel irradiance from the sun and the diffuse irradiance at the surface. A way to do this is to place a shield in the path of the sun and measure radiance with only the diffuse component. The diffuse radiance can then be subtracted from the total to determine the radiance due to the direct irradiance. It may also be possible to model some surfaces by measuring a sample in laboratory conditions. This would simplify the two above problems, but with the added concern that the laboratory sample may no longer be representative of the naturally occurring surface.

In modeling the surface of White Sands Missile Range it was decided to use an empirical model of scattering angle alone. The fit was a simple two-degree polynomial on the cosine of the scattering angle. The fit was determined from measurements at various exitant zenith and azimuth angles for a number of different incident solar zenith and azimuth angles (Deering, 1989). Measurements of the reflectance of the diffuse irradiance were not taken, and the radiance measured at any observation angle was assumed to be from the direct irradiance only, except for a constant multiplicative factor. Data were collected at three wavelengths, and at five different incident solar angles. There were 78 data points taken at each wavelength and solar incident angle. All measured values were then normalized to the reflectance at 45 degrees. The shape of the BRF was assumed to be invariant with respect to wavelength with only an overall change in magnitude. Figures 4.1, 4.2, and 4.3 show the data points taken at all sun incident angles for the wavelengths 662 nm, 826 nm, and 1658 nm. There are 390 data points per wavelength.

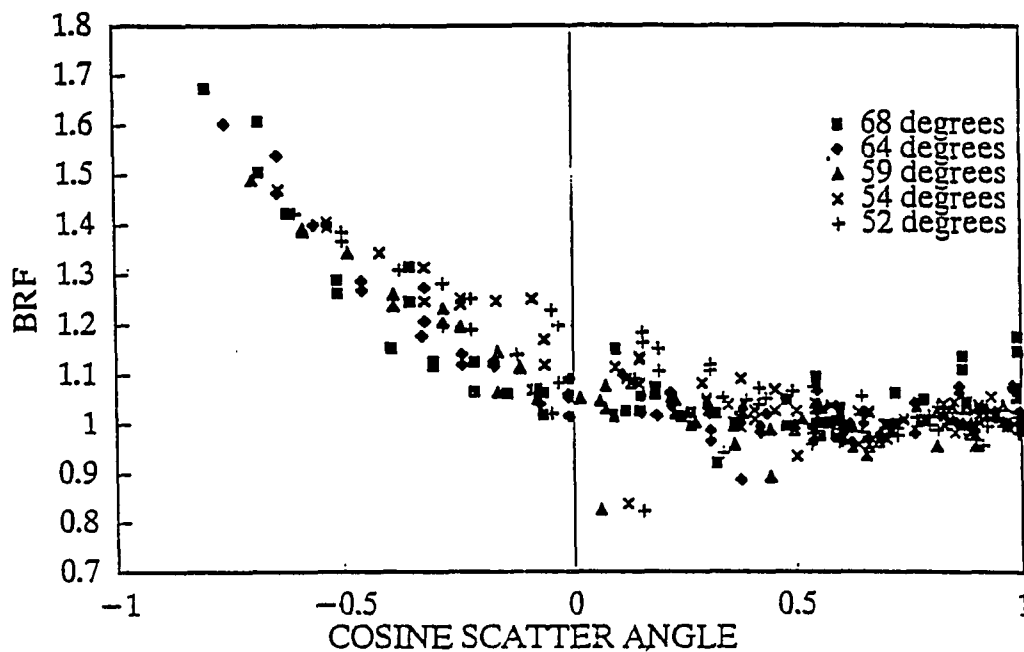


Figure 4.1: Reflectance measurements for five solar incident angles versus scattering angle for wavelength 662 nm at White Sands Missile Range. From measurements supplied by Deering.

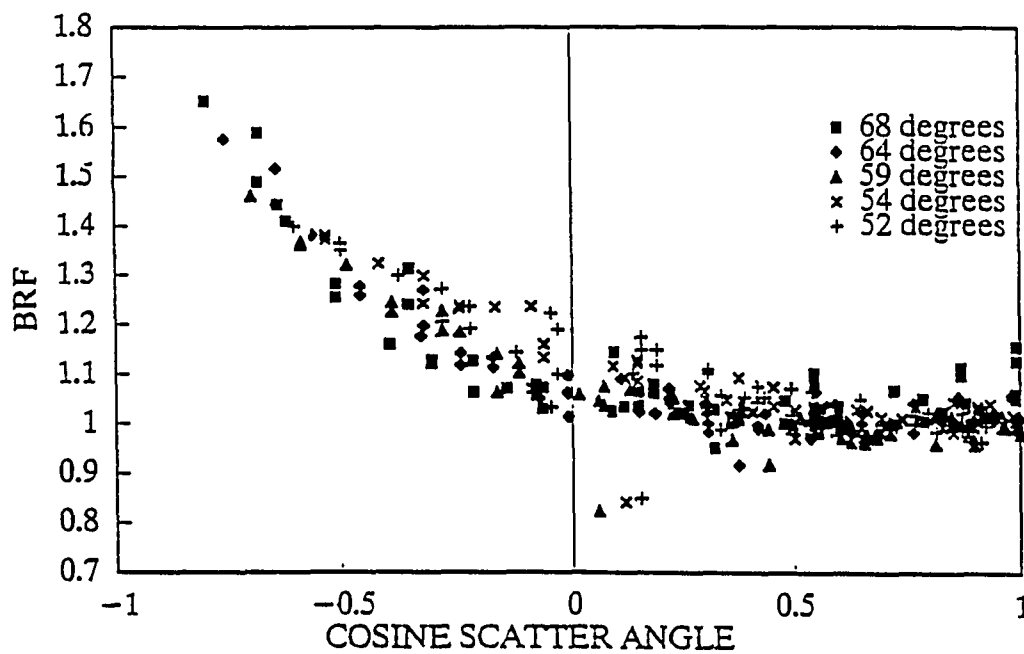


Figure 4.2: Reflectance measurements for five solar incident angles versus scattering angle for wavelength 826 nm at White Sands Missile Range. From measurements supplied by Deering.

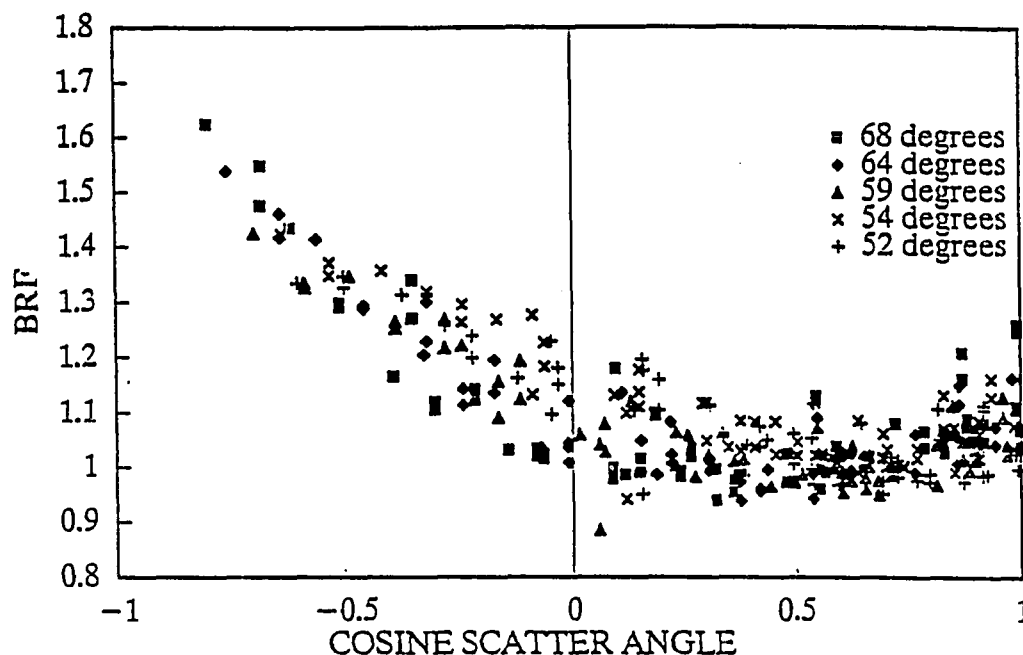


Figure 4.3: Reflectance measurements for five solar incident angles versus scattering angle for wavelength 1658 nm at White Sands Missile Range. From measurements supplied by Deering.

Figure 4.4 shows the two degree polynomial fit for each individual sun incident angle for the 662 nm wavelength measurements. The graph shows that while there may be some dependence on the incident angle, it is a relatively small effect and all incident solar zenith angles can be described by a single curve as a function of scattering angle alone.

Figure 4.5 shows the insensitivity of the model to wavelength. This graph shows the predicted two degree polynomial fit for each wavelength using all incident sun angles. The individual models match very well.

To determine the model for the BRF, every incident solar angle and wavelength measurement was used as a data point. There were a total of 1170 data points. The model fit for the reflectance was found to be

$$\text{BRF}(\mu) = 1.100 - 0.336\mu + 0.289\mu^2 \quad (4.1)$$

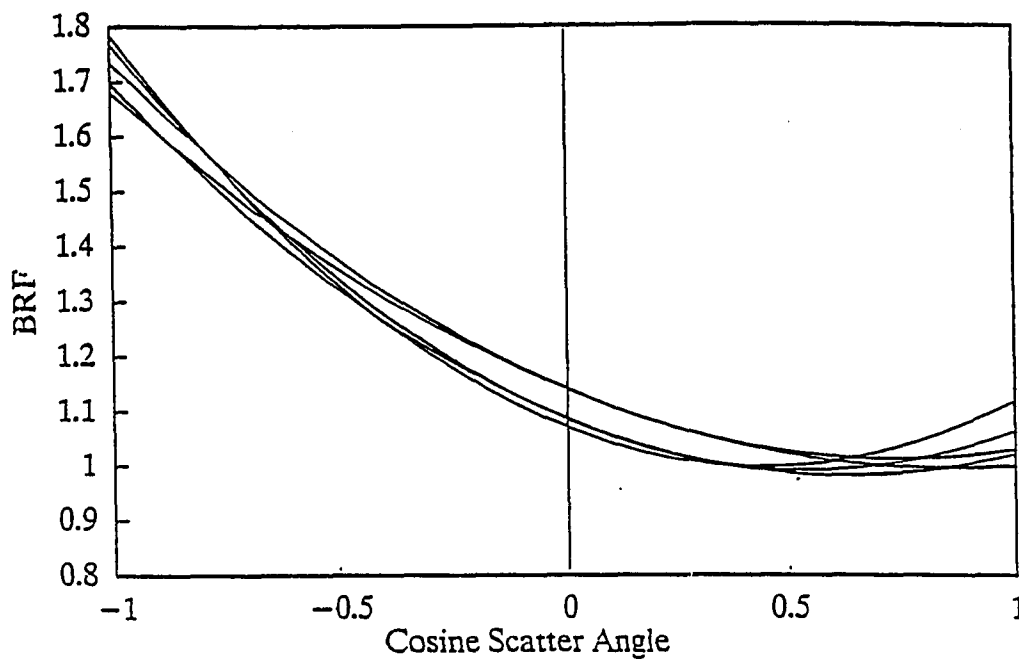


Figure 4.4: Two degree polynomial fit models for each individual sun incident angle for wavelength 662 nm.

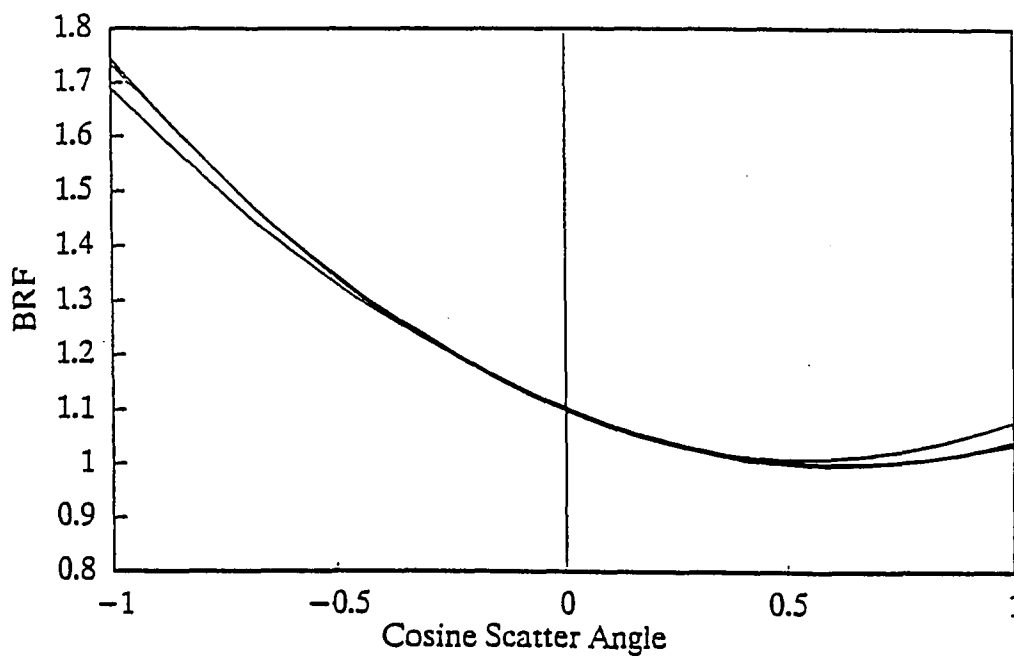


Figure 4.5: Reflectance measurements for three different wavelengths, 662 nm, 826 nm, and 1658 nm, versus scattering angle.

where the BRF is normalized to the reflectance at a scattering angle of 45 degrees and μ is the cosine of the scattering angle between the incident and exitant beams. With the standard deviation of the points assumed to be 0.05, the χ^2 value was 1168, indicating a believable fit. Variations among individual measurements would be due to the instrumentation not sampling the same surface area for each measurement, errors in the geometry, and errors due to the fact that the diffuse reflectance component is not simply some constant scale factor for the total radiance at every data point.

To use this model in a calibration, the reflectance of the surface is measured at overpass for a scattering angle between the sun and the sensor and for every wavelength of interest. The radiative transfer code then uses both the model and the scaling factor to determine the reflectance of the surface at any scattering angle. The radiative transfer code then computes the scattering angle for each incident radiance or direct irradiance component into every exitant radiance direction. As was discussed previously, the code divides the scattering into a number of discrete sections. There are ten zenith sections in both the upward and downward directions each with seven azimuthal sections. This means that there are 70 incident radiance components that scatter into 70 exitant radiance sections. The model accounts for 4900 different reflections.

Chapter 5 will show what effect the reflectance model has on the results of TM calibrations over the the previous lambertian assumption. For a surface like that of White Sands, the difference will be much less than over most surfaces. This is because the surface is very nearly lambertian over many angles. In the general problem of reflectance retrieval, the BRF models play a more important role.

CHAPTER 5

RESULTS AND CONCLUSIONS

Data have been collected for Landsat 5 TM calibrations six times since the fall of 1984: October 28, 1984, May 24, 1985, August 28, 1985, November 16, 1985, March 27, 1987, and February 10, 1988. A calibration was made at the time of the data acquisition for each day. In some cases, the data taken have been insufficient to properly perform a complete calibration. The data for each of these days have been reexamined and new calibrations performed using first the jungian method with a lambertian surface reflectance model and second the size distribution inverted from optical depth measurements with a non-lambertian surface model. Table 5.1 shows the predicted radiance values for each day, each TM wavelength, and each method.

The internal calibrator (IC) results (Barker, 1985, 1987, 1988) are determined from the digital counts due to a known irradiance level on the focal plane. They do not provide the relation between digital counts and the radiance at the entrance pupil of the system, as with the other results presented here. The radiance at the image plane can never be greater than the radiance at the entrance pupil and will most likely be less due to losses in the optics. A bias would then be expected between these results and the other calibration results, caused by system losses in the fore-optics and the change of this bias with respect to time could be an indication of the degradation of this part of the imaging system.

The methodology used in the results called "previous" in Table 5.1 and with the jungian calibration is basically the same. The dissimilar results are due to improvements made on the

Table 5.1: Predicted radiance values in $\frac{W}{m^2 \mu msr}$ for each calibration day and wavelength. The table shows, in order, the predicted value for the internal calibrator, the previous calibration results, a current calibration using the jungian size distribution with a lambertian surface model, a current calibration using a size distribution inverted from optical depth measurements with a lambertian surface model, and the inverted distribution with a non-lambertian surface reflectance model. Dashed lines indicate lack of calibrations due to insufficient data or saturated image counts.

Calibration	IC	Previous	junge	Inversion	BRDF
$\lambda = 0.4863$					
84-10-28	155.11	159.60	158.65	167.69	170.99
85-05-24	-----	244.94	237.31	249.30	250.12
85-08-28	-----	237.90	239.74	244.37	246.18
85-11-16	138.83	141.72	140.37	141.12	142.68
87-03-27	157.25	160.62	164.93	166.48	164.92
88-02-10	119.36	122.32	125.84	128.42	128.05
$\lambda = 0.5706$					
84-10-28	155.11	159.60	158.84	164.78	167.37
85-05-24	248.23	243.21	238.70	246.04	246.50
85-08-28	235.03	237.77	242.89	242.49	243.70
85-11-16	139.70	143.70	139.55	139.82	140.83
87-03-27	156.70	153.92	165.48	166.15	164.46
88-02-10	118.68	105.33	123.55	126.88	126.53
$\lambda = 0.6607$					
84-10-28	144.50	152.32	148.23	153.42	155.23
85-05-24	226.78	231.87	222.94	229.10	229.36
85-08-28	216.42	222.84	222.25	222.78	223.99
85-11-16	130.24	135.43	130.82	130.87	131.45
87-03-27	147.28	148.52	153.02	153.99	152.40
88-02-10	112.31	105.11	114.08	116.29	115.98
$\lambda = 0.8382$					
84-10-28	112.52	102.56	108.97	112.08	112.86
85-05-24	172.06	156.07	161.38	164.19	164.25
85-08-28	158.66	153.02	159.25	161.08	161.47
85-11-16	102.88	96.90	98.60	98.53	98.70
87-03-27	117.95	115.50	117.24	118.42	117.16
88-02-10	89.71	87.41	88.57	89.46	89.20

Table 5.1 (continued): Predicted radiance values in $\frac{W}{m^2 \mu m sr}$ for each calibration day and wavelength. The table shows, in order, the predicted value for the internal calibrator, the previous calibration results, a current calibration using the jungian size distribution with a lambertian surface model, a current calibration using a size distribution inverted from optical depth measurements with a lambertian surface model, and the inverted distribution with a non-lambertian surface reflectance model. Dashed lines indicate lack of calibrations due to insufficient data or saturated image counts.

Calibration	IC	Previous	junge	Inversion	BRDF
$\lambda = 1.6770$					
84-10-28	12.93	10.96	14.26	14.42	14.45
85-05-24	-----	-----	-----	-----	-----
85-08-28	20.64	18.65	22.10	22.19	22.22
85-11-16	11.95	11.31	12.56	12.53	12.53
87-03-27	13.01	13.90	14.01	14.08	13.93
88-02-10	9.01	9.87	9.97	10.05	10.03
$\lambda = 2.223$					
84-10-28	1.59	1.49	1.73	1.75	1.75
85-05-24	-----	-----	-----	-----	-----
85-08-28	2.78	2.63	2.87	2.88	2.88
85-11-16	1.32	1.33	1.42	1.41	1.41
87-03-27	1.56	1.63	1.61	1.60	1.60
88-02-10	1.03	1.13	1.14	1.15	1.14

data reduction algorithms since the calibrations were originally performed. The major change in the current jungian-based calibration versus the "previous" is the method in determining the jungian parameter. The previous method determined the jungian parameter from only two optical depth values. This was to avoid using optical depths with a contribution from ozone absorption. The problem with this method is that an error in either measurement can significantly affect the estimation of the jungian parameter. The current method solves simultaneously for the jungian parameter and the ozone concentration.

Table 5.2: Percent difference in radiance prediction between inversion-based calibration with non-lambertian surface model and jungian-based calibration with a lambertian model.

	84-10-28	85-05-24	85-08-28	85-11-16	87-03-27	88-02-10
$\lambda = 0.4863$						
total	7.21	5.12	2.61	1.62	-0.01	1.72
optical depth	-0.42	0.99	1.16	0.37	3.15	-1.08
transmittance	-0.15	-0.04	-0.41	0.00	-0.14	0.23
path radiance	2.63	2.92	0.98	0.41	0.16	1.62
diffuse ref.	2.88	1.37	0.70	-0.10	-0.86	0.69
BRF model	1.93	0.33	0.73	1.09	-0.95	-0.29
$\lambda = 0.5706$						
total	5.10	3.16	0.33	0.91	-0.62	2.36
optical depth	-0.55	0.53	1.32	0.34	2.28	-1.02
transmittance	-0.76	-0.23	-2.07	0.00	-0.68	1.14
path radiance	2.06	1.74	0.49	0.10	0.36	1.44
diffuse ref.	2.45	1.09	0.44	-0.17	-0.85	0.72
BRF model	1.55	0.19	0.50	0.72	-1.03	-0.27
$\lambda = 0.6607$						
total	4.51	2.80	0.78	0.48	-0.41	1.64
optical depth	-0.08	0.45	1.05	0.19	1.64	-0.79
transmittance	-0.44	-0.13	-1.19	0.00	-0.39	0.66
path radiance	1.63	1.34	0.28	0.02	0.53	1.22
diffuse ref.	2.06	1.12	0.30	0.15	0.75	0.60
BRF model	1.17	0.11	0.37	0.44	-1.04	-0.26
$\lambda = 0.8382$						
total	3.45	1.74	1.37	0.10	-0.07	0.71
optical depth	0.76	-1.02	0.37	-0.02	1.17	-0.37
transmittance	0.00	0.00	0.00	0.00	0.00	0.00
path radiance	0.87	1.30	0.37	0.01	0.65	0.92
diffuse ref.	1.15	1.32	0.45	-0.06	-0.63	0.70
BRF model	0.69	0.03	0.76	0.17	-1.08	-0.28

Table 5.2 (continued): Percent difference in radiance prediction between inversion-based calibration with non-lambertian surface model and jungian-based calibration with a lambertian model. Dashed lines indicate lack of radiance predictions due to insufficient data.

	84-10-28	85-05-24	85-08-28	85-11-16	87-03-27	88-02-10
$\lambda = 1.6770$						
total	1.32	----	0.52	-0.24	-0.58	0.59
optical depth	1.06	----	-0.09	-0.24	1.33	-1.76
transmittance	0.00	----	0.00	0.00	0.00	0.00
path radiance	0.11	----	0.19	0.02	0.28	1.38
diffuse ref.	-0.01	----	0.29	0.00	-1.03	0.99
BRF model	0.17	----	0.47	-0.02	-1.08	-0.26
$\lambda = 2.223$						
total	0.97	----	0.35	-0.20	-0.68	0.68
optical depth	0.73	----	0.11	-0.22	0.26	-1.80
transmittance	0.00	----	0.00	0.00	0.00	0.00
path radiance	0.18	----	0.16	0.02	1.20	1.38
diffuse ref.	-0.03	----	0.22	0.00	-0.53	0.99
BRF model	0.10	----	0.37	-0.01	0.00	-0.22

Table 5.2 shows the percent difference in predicted radiance between the calibration using the inverted size distribution and the non-lambertian surface model versus the jungian distribution and lambertian surface model calibration. A positive value represents an increase in the predicted radiance with the inverted size distribution. Table 5.2 also attempts to show the source of these differences.

The optical depth percentage is the change in radiance due to the change in predicted optical depth for each distribution. This accounts for the change in the direct irradiance at the surface and the change in attenuation of the radiance in the path from the surface directly to the sensor. This is in effect the change in the single scattering radiance due to the change in optical depth. A change in optical depth will also affect the diffuse radiance at the surface as well as the path radiance, but is considered in other terms.

The transmittance term is the change in the transmittance of the atmosphere due to absorption. As the models for most absorption species were assumed to be the same for either calibration, this difference is due to the difference in ozone concentration only. Ozone concentration is computed with the jungian distribution, but independently obtained with the inversion procedure. For the calibration with the largest difference due to this term, August 28, 1985, the predicted ozone concentration for the jungian method was 0.175 cm-atm and 0.268 cm-atm for the other. The jungian prediction falls well below the average ozone concentration of approximately 0.265 cm-atm for August at White Sands as determined by smoothed yearly data from TOMS.

The path radiance term is an estimate of the change in the intrinsic atmospheric path radiance at the sensor. This is affected by a change in optical depth and a change in the single scattering albedo or shape of the phase function of the aerosol particles. All these parameters are affected by the change in the size distribution of the aerosol particles.

The diffuse reflectance term is the change due to the diffuse radiance at the surface reflecting off the surface and into the field-of-view of the sensor. This term assumes a lambertian reflectance and is not affected by the BRF model. It is a function of the diffuse field at the surface which, like the path radiance is a function of the optical depth, single scattering albedo, and phase function shape of the aerosol particles.

The BRF term is the change brought about by the inclusion of the non-lambertian surface reflectance model. The percentage was obtained by running the radiative transfer code both with and without the surface model and comparing the results.

It should be noted that the sum of the individual percentage values does not exactly equal the total change. This is because these percentages are approximations based primarily on single and double scattering events. The difference between the factors is due to more complicated scattering events. Also, the largest differences between the two methods are in the shortest wavelengths as previously predicted.

The internal calibration for TM is based on a moving flag which directs an internal source of radiance directly onto the focal plane. The flag is also used to determine the number of counts recorded when no radiance is incident on the focal plane. This offset should be the same for each calibration procedure. To obtain the number of digital counts per unit radiance, the offset determined by the IC is subtracted from the recorded number of scene digital counts and this value is divided by the radiance predicted by each calibration technique to obtain the counts per unit radiance. This assumes a linear response for the sensor. These values are shown for each TM band in Figures 5.1 through 5.6. May 24, 1985 was omitted because the optical depths for this day were determined from inadequate data and are unreliable. The IC calibrations are for counts per unit radiance on the image plane and should be higher than those predicted by the other calibration methods.

The lower three TM bands give reasonable results in terms of the reflectance-based methods in comparison with the IC results. The non-jungian distribution seems to predict a counts per radiance that is too low for the calibration on October 28, 1984. This may be due to the fact the non-jungian size distribution predicts a much greater amount of diffuse radiance than the jungian distribution. Measurements of the actual diffuse radiance are not available for this day. The calibration on November 16, 1985 gives strange results, as well. Both calibration methods predict a jump in the counts per unit radiance for TM bands 1 through 5. This

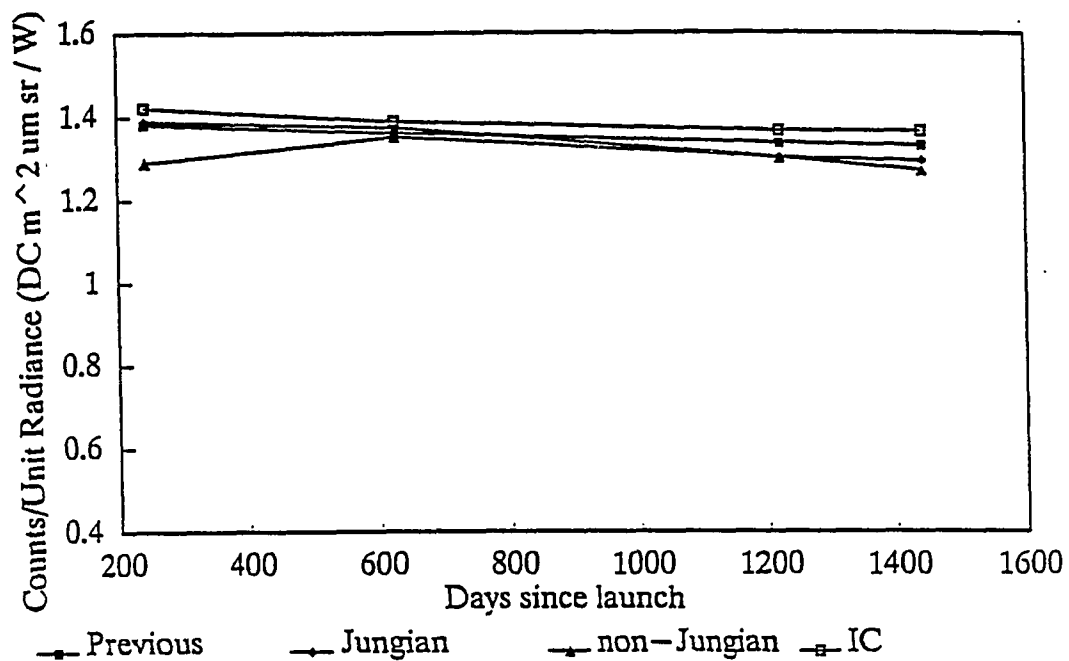


Figure 5.1 : Predicted counts per unit radiance for TM band 1 with $0.4863 \mu\text{m}$ center wavelength. The calibration on August 28, 1985 is missing due to the fact that the band was saturated during overpass.

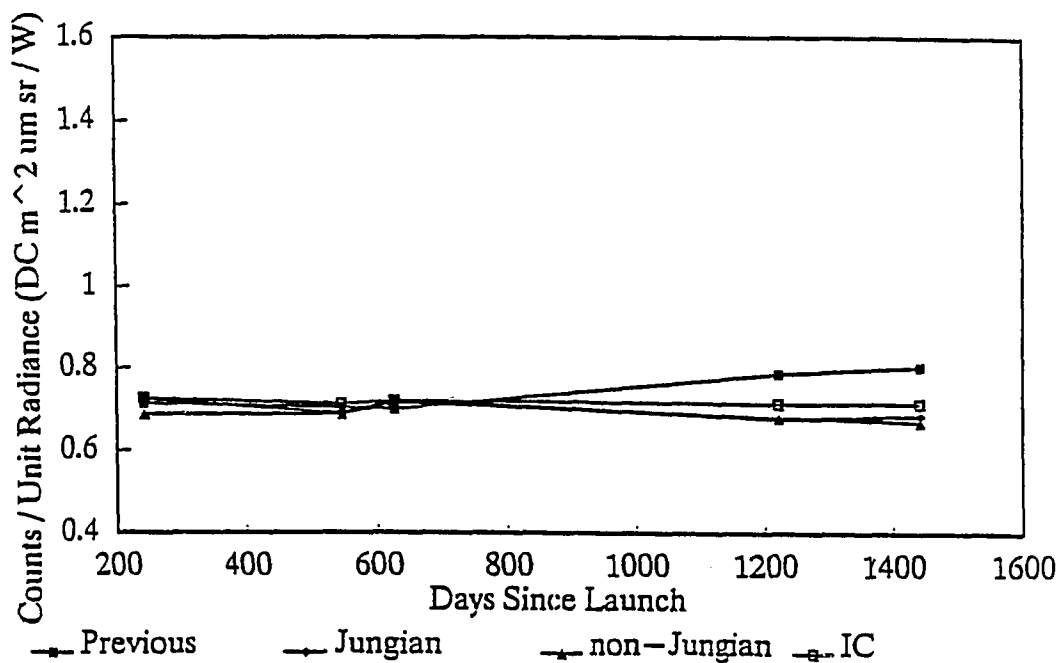


Figure 5.2 : Predicted counts per unit radiance for TM band 2 with $0.5706 \mu\text{m}$ center wavelength.

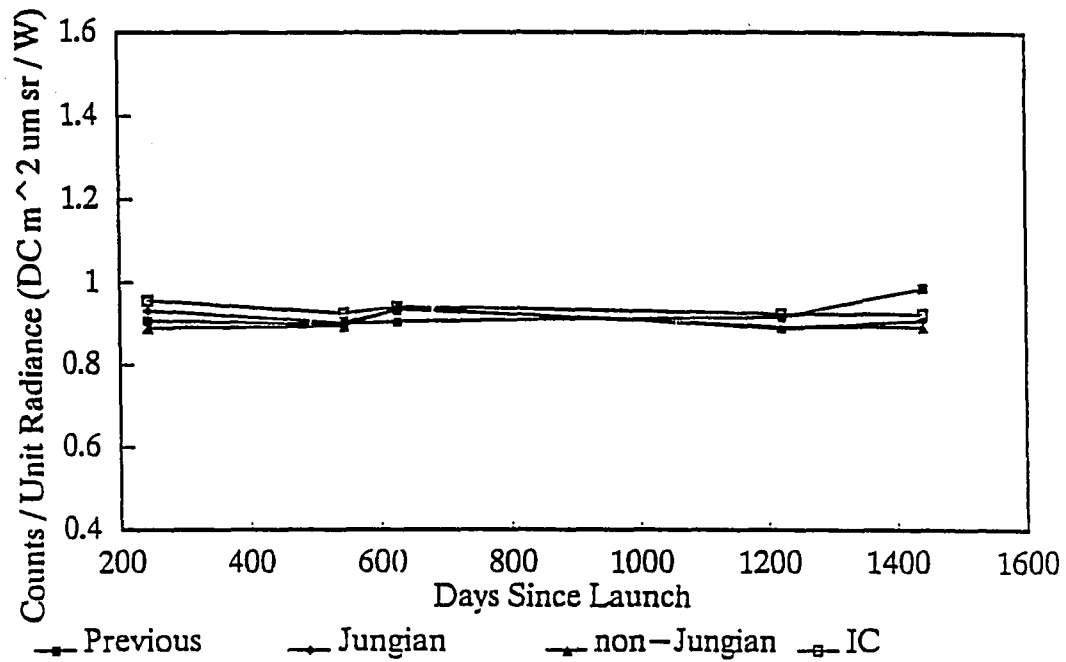


Figure 5.3 : Predicted counts per unit radiance for TM band 3 with $0.6607 \mu\text{m}$ center wavelength.

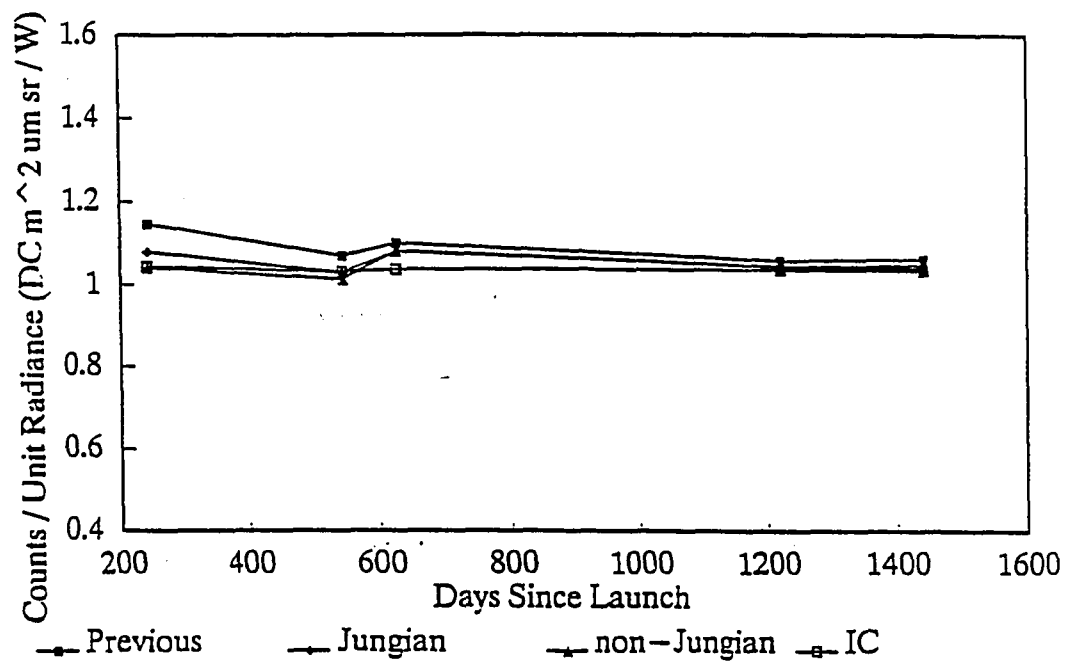


Figure 5.4 : Predicted counts per unit radiance for TM band 4 with $0.8382 \mu\text{m}$ center wavelength.

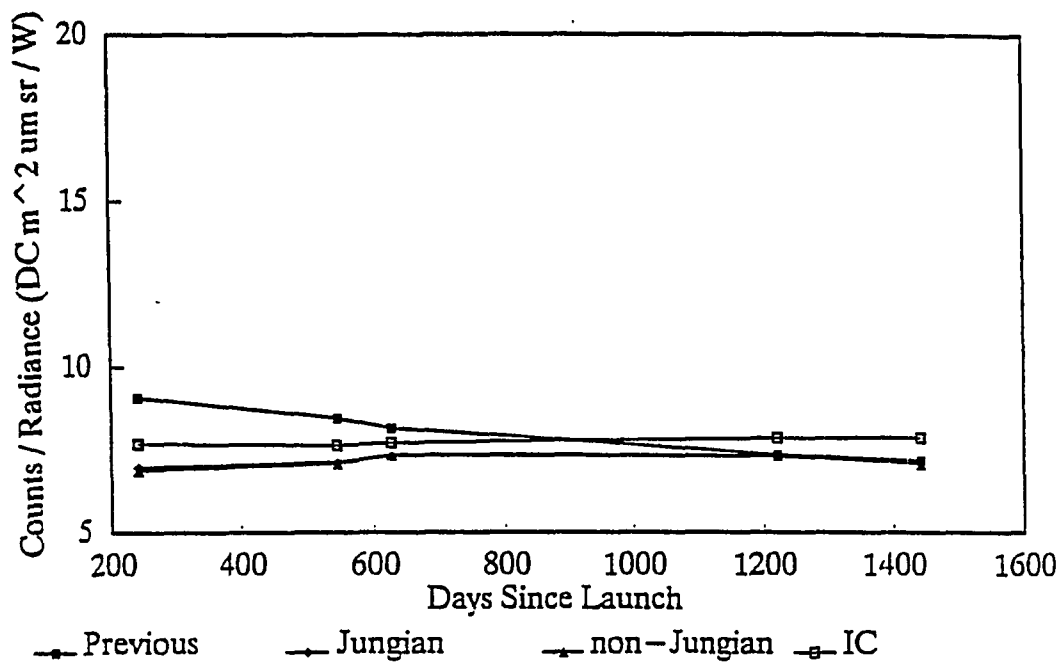


Figure 5.5 : Predicted counts per unit radiance for TM band 5 with 1.677 μm center wavelength.

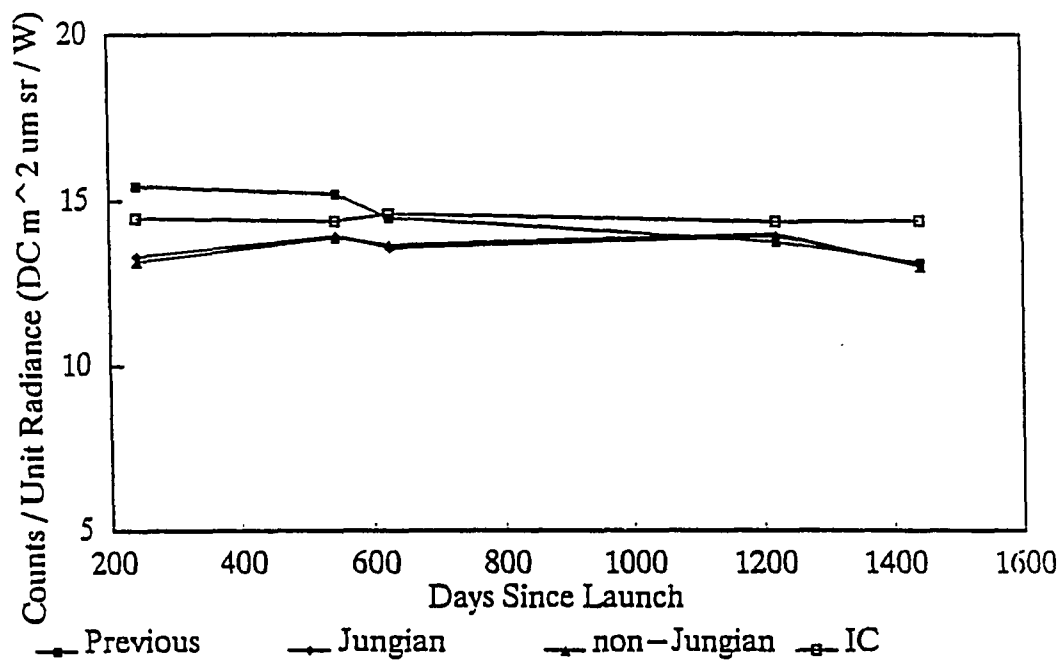


Figure 5.6 : Predicted counts per unit radiance for TM band 7 with 2.223 μm center wavelength.

could be due to a systematic error in both reflectance-based methods for this particular day. It was thought the day was so exceptionally clear that the radiance was not sufficiently depolarized by the aerosols, resulting in an error due to the non-polarization code. Using the polarization version of the Herman code for this day changed the predicted radiance at the sensor by less than 0.2 percent. Therefore, the non-polarization code is still reasonably accurate. The fact that the day was so clear has another effect, which is the optical depths for the higher wavelengths were too small to be measured accurately. The lack of these measurements make it more difficult to determine a size distribution.

Another interesting feature of the November 16th calibration is that the IC predictions increase significantly as well. If this increase is accurate, then some of the increase in the reflectance-based methods is due to a change in the sensor itself. Since the increase is considerably greater in the reflectance-based calibrations, more than one problem may be present.

TM band 4 is the only band for which the calibrations consistently predict a counts per unit radiance higher at the entrance pupil than at the focal plane. This is most likely caused by a systematic error either in the reflectance-based or IC calibrations, or in the preflight characterization of this band. The most likely possibility is that the attenuation due to water vapor is over estimated for this band. Another possibility is that the bandpass has changed. This would affect the reflectance-based calibrations differently than the IC calibrations.

The final two TM bands are well behaved though neither show a smooth change over time. The major problem for these bands is that the optical depths for each are not well determined, having to be extrapolated from optical depth measurements ending near $1 \mu\text{m}$. Also, the responses of these bands are affected by cyclic "outgassings" of the sensor (Barker, 1985).

Table 5.2 is helpful in determining the usefulness of replacing the lambertian surface reflectance with a reflectance model. In Chapter 3 it was shown that the basic surface reflectance model replicated the surface BRF reasonably well and decidedly better than the lambertian assumption, especially in the oblique reflections of the diffuse radiance. Table 5.2 shows that this model does affect the outcome of the calibration, varying nearly two percent from the lambertian surface results in the most notable case. The effect of the surface reflection model is generally stronger in the shorter wavelengths, because of the larger role of the diffuse field radiance on the calibrations in this wavelength region. Inclusion of the surface reflectance model should reduce the errors due to the surface reflection by up to two percent, resulting in an overall error of two percent due to measurement error, inhomogeneity and variations from the BRF model. Improvement on the BRF model might include taking BRF measurements under different environmental conditions, such as various relative humidities, to determine the effect of these parameters on the surface reflection. A more complex reflection model such as developed by Hapke (1981) might improve calibrations, though the simpler model seems to fit the available data very well.

Whether or not the inclusion of the size distribution inverted from optical depth measurements improved calibration procedures over the jungian distribution method is less clear. As stated previously, the entries under optical depth, path radiance, and diffuse reflectance in Table 5.2, are all affected primarily by the change of the size distribution between the two methods. One possible validation of each distribution is to compare how each predicts the optical depths at the wavelengths for which data were taken. The problem is that for the jungian distribution, the iterative routine to simultaneously determine the jungian parameter and the ozone concentration effectively forces the optical depth measurements to be more jungian. In calibrations where TOMS data are not available, a method to determine the ozone

concentration from the optical depth measurements without assuming a jungian distribution could be used to determine the ozone concentration for both methods. Then a comparison of predicted versus measured Mie optical depths could be made for the two distributions.

The distributions affect more than the optical depth, however. The single scattering albedo and shape of the phase function change as well. Since both of these affect the diffuse radiance at the ground, another method to determine the more accurate distribution would be to compare the diffuse-to-global radiance ratio predicted by each distribution to the actual measured values for this ratio. Figures 5.7 through 5.10 are graphs of these ratios for all calibration days and wavelengths for which these measurements were recorded. The figures do not indicate that one distribution consistently predicts a more accurate diffuse to global ratio. Valuable information is still available in these figures. Examination of these ratios in conjunction with the calibration results for these days show a correlation between the errors in this ratio and errors in the final calibrations. For example, the predicted ratio for November 16, 1985 is less than measured for TM bands 2 through 5. This corresponds to the low radiance predictions at the sensor. An increase in the diffuse field would mean an increase in the radiance at the sensor and a decrease in the predicted counts per unit radiance. The diffuse-to-global ratio is influenced mostly by the single scattering albedo of the phase function. This, in turn, is affected by the index of refraction and radii limits of the aerosols. Repeated attempts to adjust the limits of the size distribution and the non-dispersive index for this date could not replicate the measured ratio. This includes an attempt with particles with no absorption, implying a single scattering albedo of unity. The failure of the computed size distribution in predicting the measured diffuse-to-global at the surface is a good indication that the phase function is not representative of the actual scattering and will result in errors in the predicted radiance.

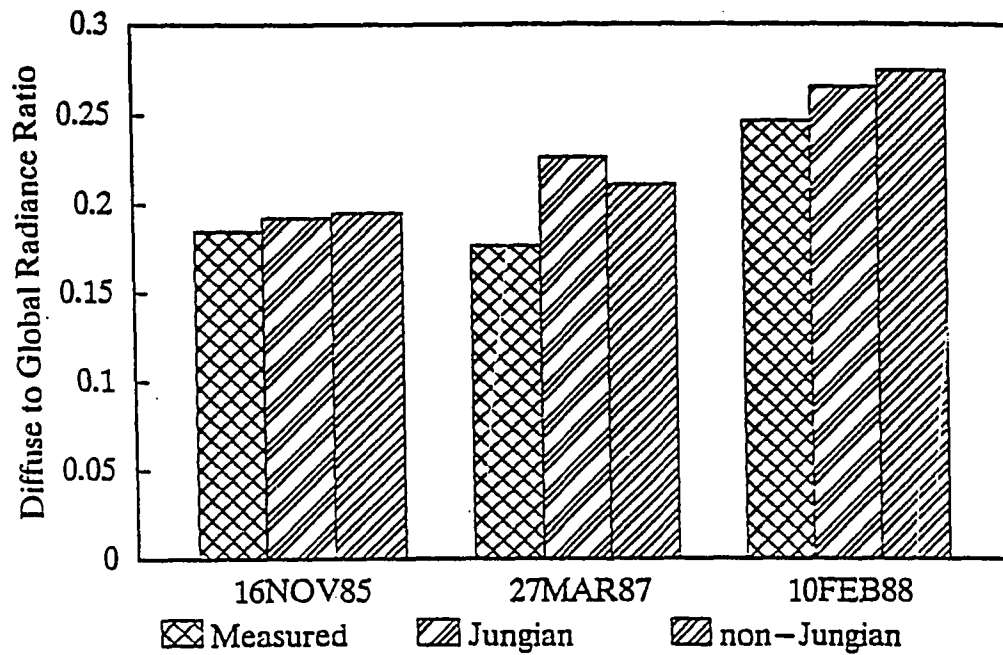


Figure 5.7 : Diffuse to Global radiance ratios, predicted and measured values for $0.4863 \mu\text{m}$.

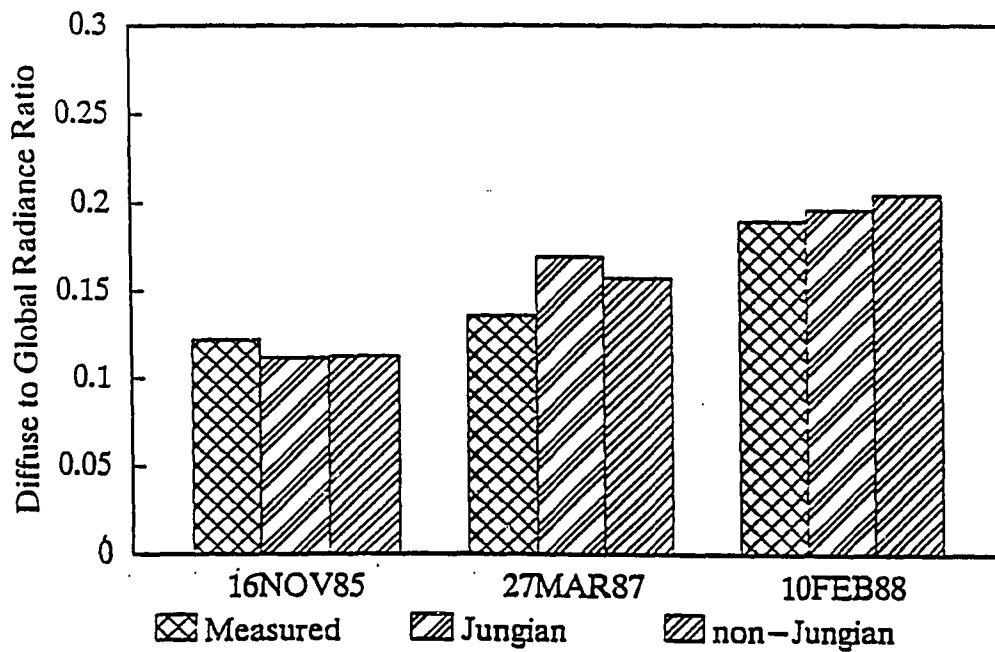


Figure 5.8 : Diffuse to Global radiance ratios, predicted and measured values for $0.5706 \mu\text{m}$.

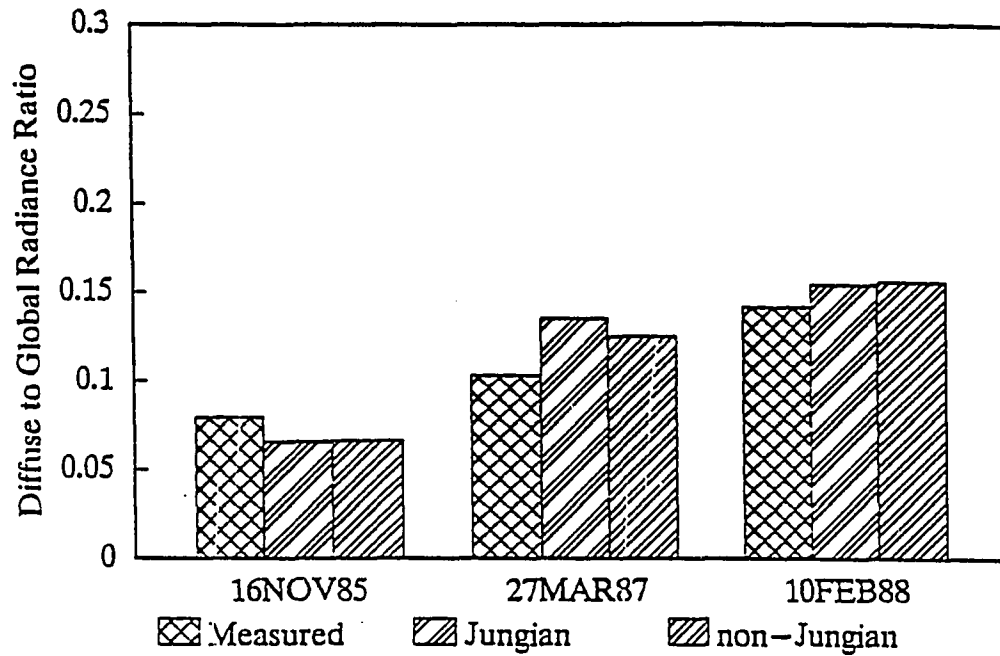


Figure 5.9 : Diffuse to Global radiance ratios, predicted and measured values for $0.6607 \mu\text{m}$.

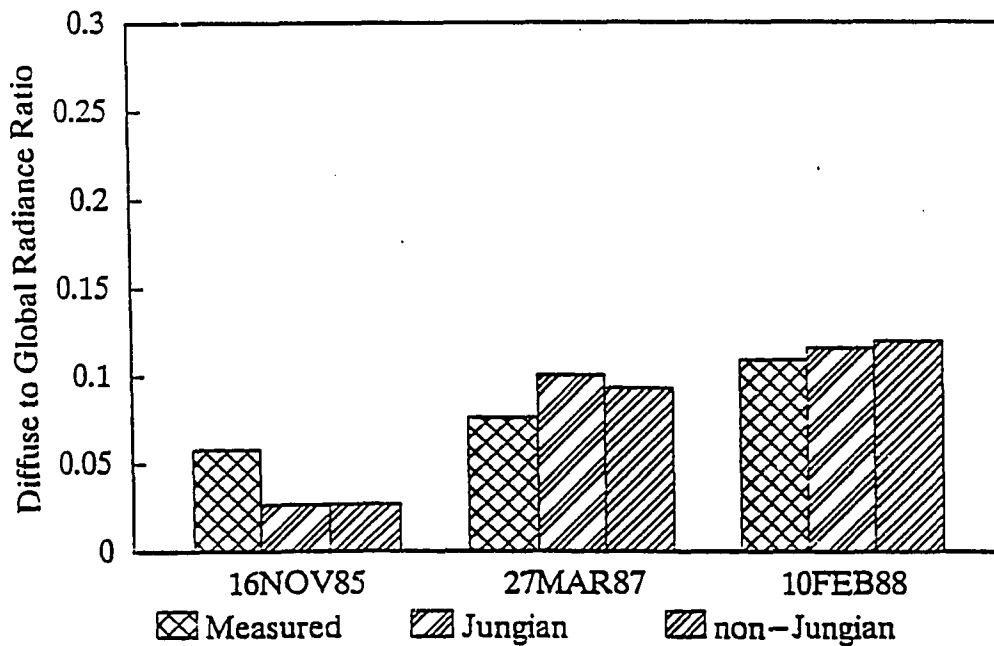


Figure 5.10 : Diffuse to Global radiance ratios, predicted and measured values for $0.8382 \mu\text{m}$.

For a simple model of the change in counts per unit radiance over a time, a straight line fit of the data points was found for each TM band. This was done by a simple least-squares fit of the data for the non-lambertian method with BRF correction and for the IC. These results are shown in figures 5.10 through 5.15. All calibrations were included except for the May 24, 1985 calibration and the October 28, 1984 point in TM band 1 which skewed that fit greatly from the other data points. The slope and intercept for these lines are shown in table 5.3.

Table 5.3 : Linear fit slopes and intercepts

	TM 1	TM 2	TM 3	TM 4	TM 5	TM 7
IC slope	-4.7e-5	-5.6e-6	-2.2e-5	-3.4e-6	1.9e-4	-1.1e-4
intercept	1.4263	0.7264	0.9513	1.0383	7.5966	14.510
non-jung. slope	-9.5e-5	-1.7e-5	-4.9e-6	1.1e-5	2.2e-4	-5.8e-5
intercept	1.4120	0.7021	0.9041	1.0243	6.9062	13.566

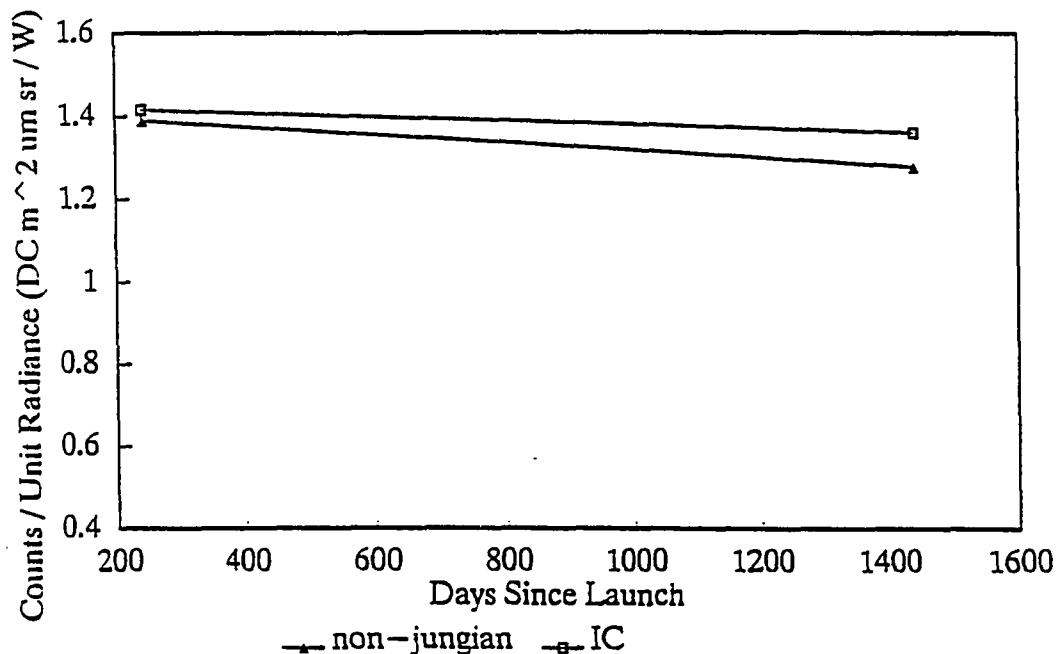


Figure 5.11 : Straight line fit of non-jungian, and IC counts per unit radiance for TM band 1 with $0.4863 \mu\text{m}$ center wavelength.

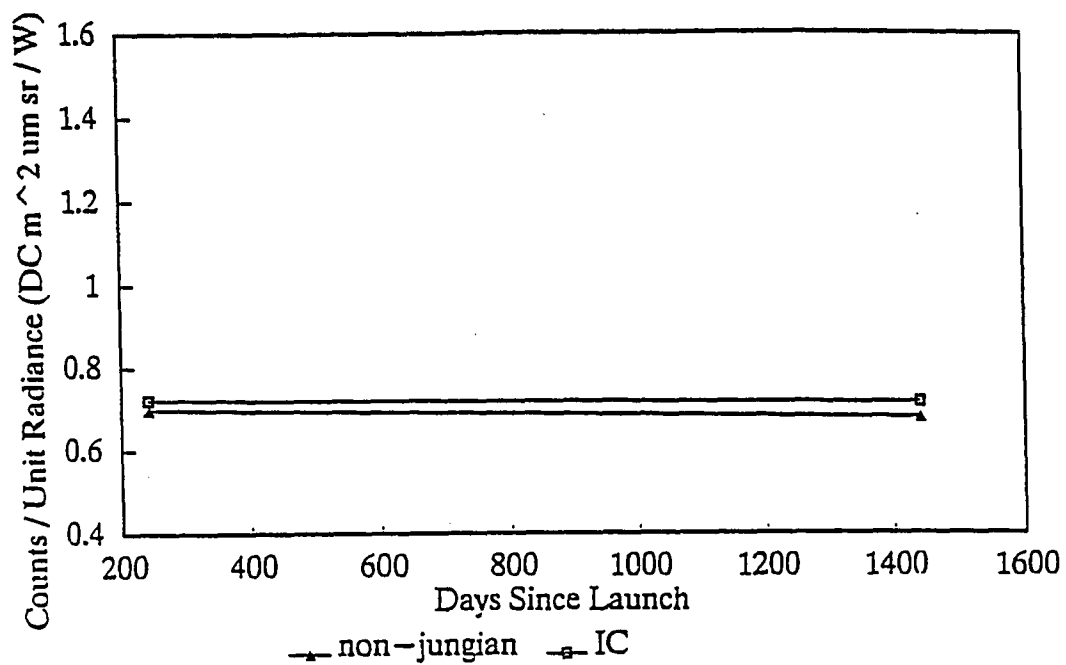


Figure 5.12 : Straight line fit of non-jungian, and IC counts per unit radiance for TM band 2 with 0.5706 μm center wavelength.

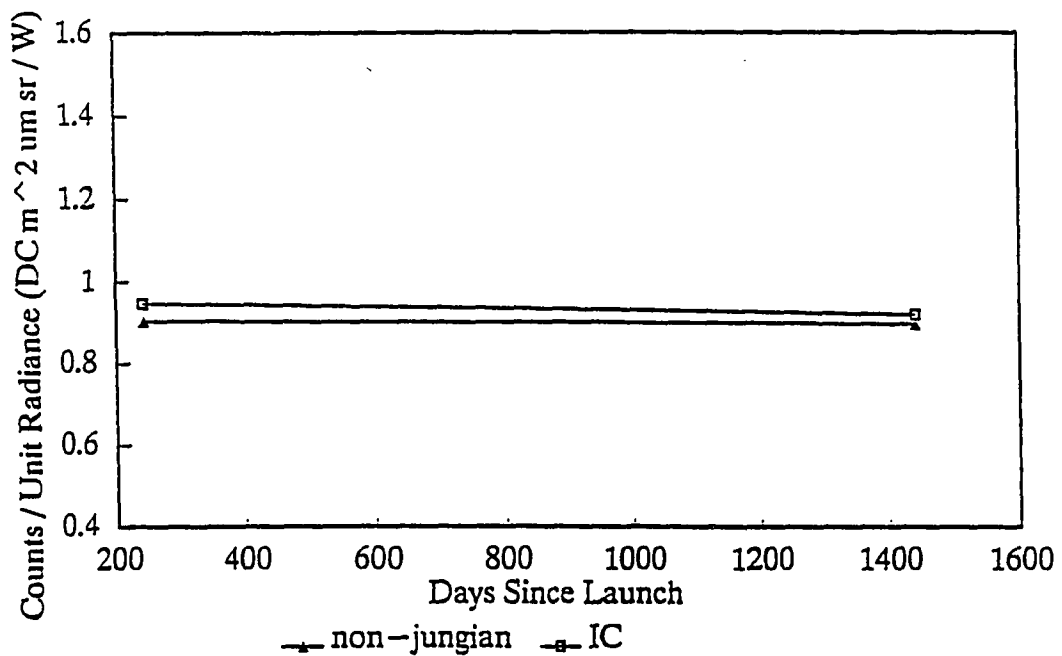


Figure 5.13 : Straight line fit of non-jungian, and IC counts per unit radiance for TM band 3 with 0.6607 μm center wavelength.

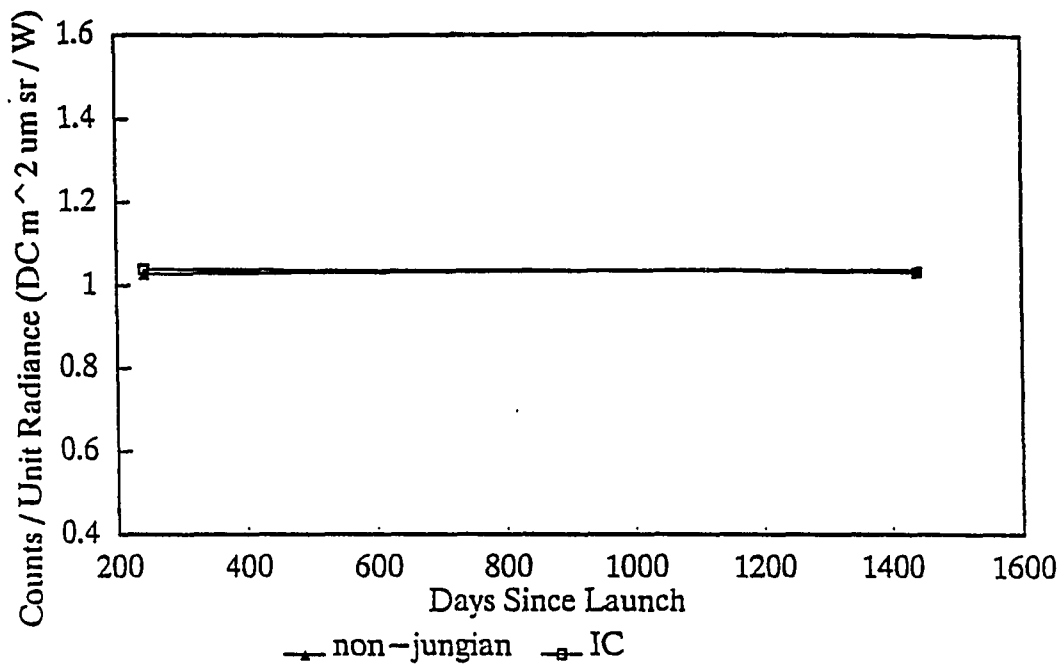


Figure 5.14 : Straight line fit of non-jungian, and IC counts per unit radiance for TM band 4 with $0.8382 \mu m$ center wavelength.

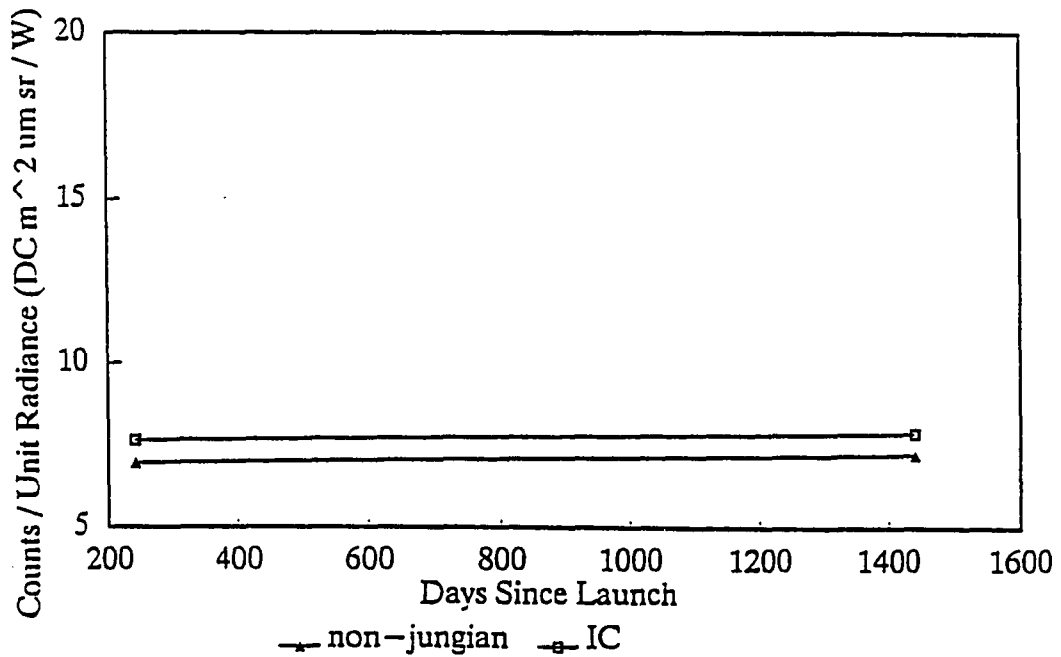


Figure 5.15 : Straight line fit of non-jungian, and IC counts per unit radiance for TM band 5 with $1.677 \mu m$ center wavelength.

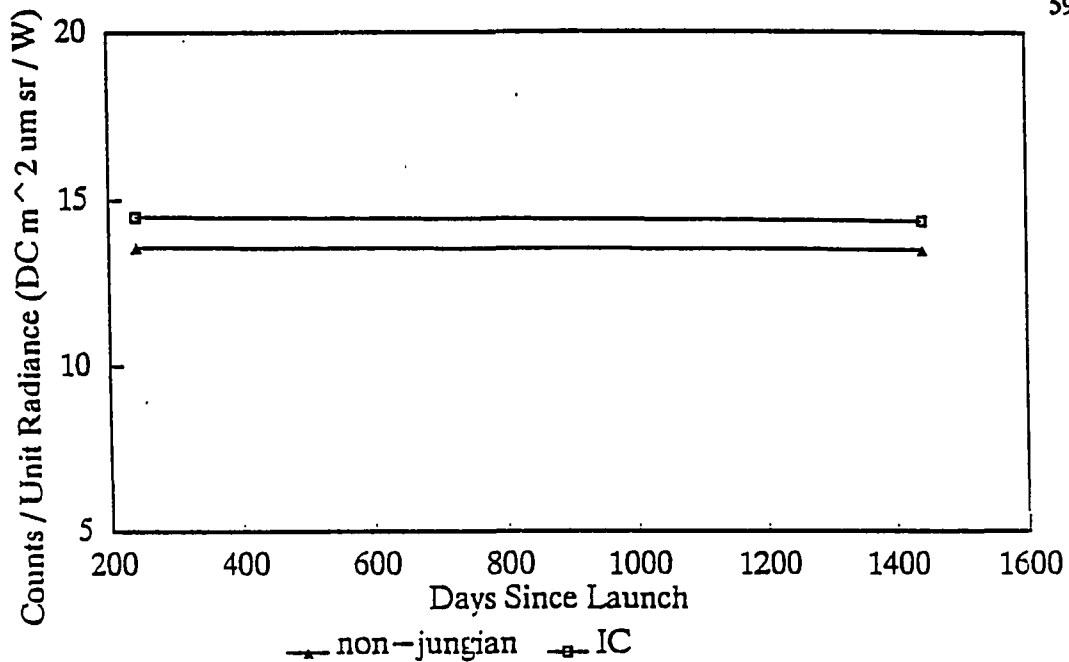


Figure 5.16 : Straight line fit of non-jungian, and IC counts per unit radiance for TM band 7 with 2.223 μm center wavelength.

There are a number of possibilities to increase the accuracy of the reflectance-based calibrations. The measurements of the optical depth should extend out to the wavelength region of TM band 7. The increased data will be very useful for predicting optical depths for bands 5 and 7 more accurately. Since the number of scattering events decreases with increasing wavelength, a direct solar transmission and reflectance model becomes more accurate making the optical depth the major atmospheric parameter in predicting the radiance at the sensor. Considerations of the diffuse field, path radiance, etc, become less important for these longer wavelengths. Also, an increase in the number of measurements of optical depth will help in the determination of the size distribution, regardless of whether it is a jungian assumption or an inversion.

It is also clear that how well the aerosols predict the diffuse-to-global ratio at the surface is

important in performing accurate calibrations. Errors up to three percent in reflected radiance can be attributed to an inaccurate prediction of this ratio. In future calibrations, particular attention should be paid to this ratio in determining the validity of the aerosol distribution. This might include adjusting the index of the particles or the radius range to obtain a more accurate model. A method that would simultaneously find the size distribution and the index of refraction of the particle using a combination of the optical depths and the diffuse to global ratios would be ideal.

It is possible that no distribution of spherical particles can simultaneously produce the given optical depths and diffuse to global ratios. This could be because the actual aerosol particles might not scatter light like spherical particles. One solution to this would be to measure the phase function directly and avoid the intermediate steps of determining a size distribution and index for the particles and calculating the scattering. This would most likely be attempted by making measurements on the solar aureole. If the diffuse to global measurements could be used to obtain the single scattering albedo, then the phase function could be determined for input into the Herman code without any need to characterize the aerosols any further. This method could reduce a large number of the assumptions currently required.

APPENDIX A

CALIBRATION PROGRAM

Figure A.1 is a flowchart of the steps that are necessary to complete a calibration. Each camfered box in the flowchart represents a data reduction algorithm requiring a different computer program to complete. The squared boxes represent data input. One difficulty in completing a calibration has been in preparing the data from any one program for its use as input in the next program. The major reason for this is that the individual programs have been collected from various sources. There is no inherent compatibility between the programs and the various input and output schemes, user interfaces, and even computer language varies from program to program. A great portion of the calibration involved manually preparing the data from one program so as to be useful for the next program. The newly developed computer program was developed to assist in this part of the entire procedure. The program consists of two main parts. The first part is designed to provide the user with a method of entering the data for each program in a simple and consistent manner, and then to prepare a large batch file to run the program set desired. The method allows the user to prepare the calibration in a somewhat interactive environment, determining all parameters at one time, and the batch file technique means that the user does not have to wait for the routines to actually run, as they can take quite some time. Using this program, the user could prepare a number of separate calibrations and let them complete over night or at any other convenient time. The second part of the program is to provide routines which prepare the data from one computer output as input for the next computer program. Removing the manual step between each program increases the speed of a calibration and reduces the possibility of errors.

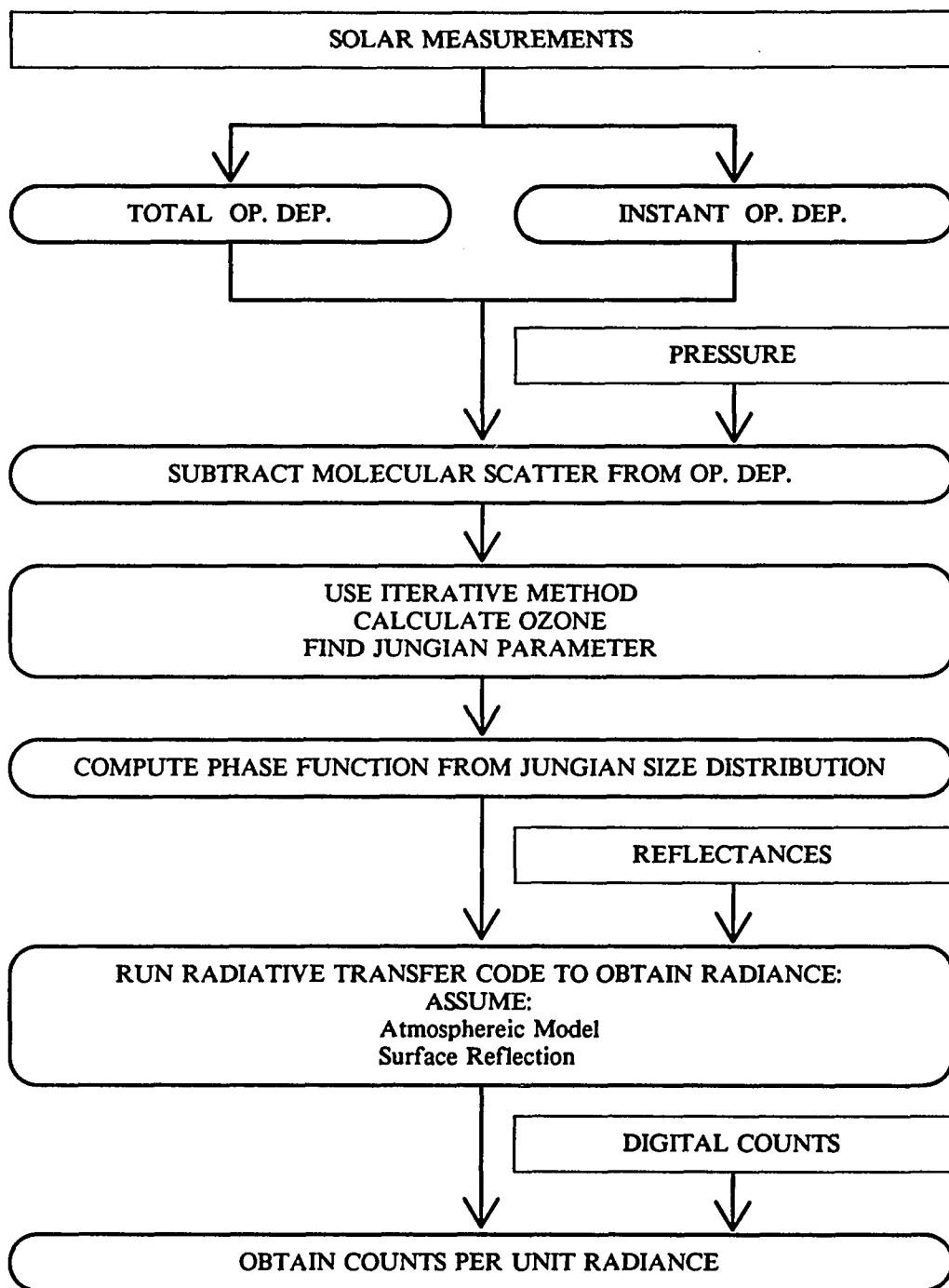


Figure A.1: Calibration overview

The problem with the method employed is that the program is entirely dependent on the fact that each individual program remain exactly the same. Any changes made in any program's input or output will necessitate a change in the overall calibration program.

LIST OF REFERENCES

- Barker, J. L. (1985), Relative radiometric calibration of Landsat TM reflective bands, *Landsat-4 Science Characterization Early Reports, NASA Conf. Pub. 2355, Part 2*, 3:1-219.
- Barker, J. L., and R. Kumar (1985), Landsat 5 White Sands 28AUG85, *Trapp 50545-17084*, Goddard Space Flight Center, Flight Dynamics Division, Greenbelt, Maryland.
- Barker, J. L., R. Kumar, and J. Wang (1987), Landsat 5 White Sands GMT=17:01:18 27MAR87, *Trapp 51121-17013*, Goddard Space Flight Center, Flight Dynamics Division, Greenbelt, Maryland.
- Barker, J. L., R. Kumar, and J. Wang (1988), Landsat 5 White Sands GMT=17:07:24 16NOV85, *Trapp 50625-17074*, Goddard Space Flight Center, Flight Dynamics Division, Greenbelt, Maryland.
- Barker, J. L., R. Kumar, and J. Wang (1988), Landsat 5 White Sands GMT=17:09:06 28OCT84, *Trapp 50241-17091*, Goddard Space Flight Center, Flight Dynamics Division, Greenbelt, Maryland.
- Bartell, R. J. (1987), *Atmospheric corrections for in-flight satellite radiometric calibration*, M.S. Thesis, University of Arizona, 100 pp.
- Biggar, S. F. (1990), *In-flight methods for satellite sensor absolute radiometric calibration*, Ph.D. Dissertation, University of Arizona, 153 pp.
- Biggar, S. F. (1990), Personal Communication, Remote Sensing Group, Optical Sciences, University of Arizona.
- Bohren C. F. and D. R. Huffman (1983), *Absorption and Scattering of Light by Small Particles*, John Wiley & Sons, Inc., New York, 530 pp.
- Castle, K. R. (1985), *Absolute Radiometric Calibration of a Spectropolarimeter*, Ph.D. Dissertation, University of Arizona, 129 pp.
- Chandrasekhar, S. (1950), *Radiative Transfer*, Oxford University Press, New York. Also Dover Publications, New York (1960), 393 pp.
- Deering, D. W. (1986), A sphere-scanning radiometer for rapid directional measurements of sky and ground radiance, *Remote Sens. Environ.* 19:1-24.
- Deering, D. W. (1989), Personal Communication through Dr. P. N. Slater, Earth Sciences Branch / 623, NASA Goddard Space Flight Center, Greenbelt, Maryland.

- Deirmendjian, D. (1969), *Electromagnetic Scattering on Spherical Polydispersions*, American Elsevier, New York.
- Hapke, B. (1981), Bidirectional reflectance spectroscopy. 1. Theory, *J. Geophys. Res.* 86:3039-3054.
- Herman, B. M. (1963), *A numerical solution to the equation of radiative transfer for particles in the Mie region*, Ph.D. Dissertation, University of Arizona, 130 pp.
- Herman, B. M. (1987), Personal Communication through Dr. P. N. Slater, Department of Atmospheric Sciences, University of Arizona.
- Herman, B. M. (1989), Personal Communication, Department of Atmospheric Sciences, University of Arizona.
- Holm, R. G., M. S. Moran, R. D. Jackson, P. N. Slater, B. Yuan, S. F. Biggar (1989), Surface reflectance factor retrieval from Thematic Mapper data, *Remote Sens. Environ.*, 27:47-57.
- Iqbal, M. (1983), *An Introduction to Solar Radiation*, Academic Press, New York.
- Irons, J. R., R. A. Weismiller, and G. W. Peterson (1989), Soil reflectance, *Theory and Applications of Optical Remote Sensing*, Ghassem Asrar, ed., John Wiley & Sons, New York, 734 pp.
- Junge, C. E. (1963) *Air Chemistry and Radioactivity*, Academic Press, New York.
- Kastner, C. J. (1985) *In-flight calibration of the Landsat thematic mapper*, Ph.D. dissertation, University of Arizona.
- King, M. D., D. M. Byrne, B. M. Herman, and J. A. Reagan (1978), Aerosol size distributions obtained by inversion of spectral optical depth measurements, *J. Atmos. Sci.* 35:2153-2167.
- Liou, K. (1980), *An Introduction to Atmospheric Radiation*, Academic Press, Orlando, 392 pp.
- Mie, G. (1908), A contribution to the optics of turbid media, especially colloidal metallic suspensions, *Ann. Phys.* 25:377-445, In German.
- Palmer, J. M. (1984), Effective bandwidths for Landsat-4 and Landsat-D multispectral scanner and thematic mapper subsystems, *IEEE Trans. Geosci. Remote Sensing GE-22(3)*:336-338.
- Santer, R. P. (1987), Personal Communication through Dr. P. N. Slater, visiting scientist, Remote Sensing Group, Optical Sciences, University of Arizona.
- Slater, P. N. (1980), *Remote Sensing Optics and Optical Systems*, Addison-Wesley, Reading, Massachusetts, 575 pp.

Slater, P. N., S. F. Biggar, R. G. Holm, R. D. Jackson, Y. Mao, M. S. Moran, J. M. Palmer, and B. Yuan (1986), Absolute calibration of the thematic mapper, *Proc. SPIE* 660:2-8.

Slater, P. N., S. F. Biggar, R. G. Holm, R. D. Jackson, Y. Mao, M. S. Moran, J. M. Palmer, and B. Yuan (1987), Reflectance- and radiance-based methods for the in-flight absolute calibration of multispectral sensors, *Remote Sens. Environ.* 22:11-37.